Geomorphological effectiveness of floods to rework gravel bars: insight from hyperscale topography and hydraulic modelling

Reid HE[1], Williams RD[2*], Brierley GJ[3], Coleman SE[4] , Lamb R[5,6], Rennie CD[7] and Tancock MJ[8]

[1]*Scottish Environment Protection Agency, Stirling, UK*

[2]*Geographical and Earth Sciences, University of Glasgow, UK*

[3] *School of Environment, University of Auckland, New Zealand*

[4]*Department of Civil and Environmental Engineering, University of Auckland, New Zealand*

[5]*JBA Trust, Skipton, UK*

[6]*Lancaster Environment Centre, Lancaster University, UK*

[7]*Department of Civil Engineering, University of Ottawa, Canada*

[8]*JBA Consulting, Skipton, UK*

**Corresponding author: richard.williams@glasgow.ac.uk*

This article has been accepted for publication and undergone full peer review but has not been through the copyediting, typesetting, pagination and proofreading process which may lead to differences between this version and the Version of Record. Please cite this article as doi: 10.1002/esp.4521

Abstract

Bars are key morphological units in river systems, fashioning the sediment regime and bedload transport processes within a reach. Reworking of these features underpins channel adjustment at larger scales, thereby acting as a key determinant of channel stability. Despite their importance to channel evolution, few investigations have acquired spatially continuous data on bar morphology and sediment-size to investigate bar reworking. To this end, four bars along a 10 km reach of a wandering gravel-bed river were surveyed with Terrestrial Laser Scanning (TLS), capturing downstream changes in slope, bed material size and channel planform. Detrended standard deviations (σ_z) were extracted from TLS point clouds and correlated to underlying physically measured median grain-size (D_{50}), across a greater range of σ_z values than have hitherto been reported. The resulting linear regression model was used to create a 1 m resolution median grain-size map. A fusion of airborne LiDAR and optical-empirical bathymetric mapping was used to develop reach-scale Digital Elevation Models (DEMs) for rapid two-dimensional hydraulic modelling using JFlow® software. The ratio of dimensionless shear stress over critical shear stress was calculated for each raster cell to calculate the effectiveness of a range of flood events (2.33 - 100 year recurrence intervals) to entrain sediment and rework bar units. Results show that multiple bar forming discharges exist, whereby frequent flood flows rework tail and back-channel areas, whilst much larger, less frequent floods are required to mobilise the coarser sediment fraction on bar heads. Valley confinement is shown to exert a primary influence on patterns of bar reworking. Historical aerial photography, hyperscale DEMs and hydraulic modelling are used to explain channel adjustment at the reach scale. The proportion of the bar comprised of more frequently entrained units

(tail, back channel, supra-platform) relative to more static units (bar head) exerts a direct influence upon geomorphic sensitivity.

Key Words: bar sedimentology, wandering gravel-bed river, fluvial morphodynamics, sediment entrainment, terrestrial laser scanning.

1. Introduction

Interpreting the process-form relationship of bar complexes is a fundamental aim in fluvial geomorphological enquiry (Bluck, 1979, Church and Jones, 1982, Bridge, 2003). Bar topography and grain-size composition underpins insights into the mechanisms of channel adjustment, reach-scale sediment regime and bedload transport. Evidence for these linkages are especially apparent in wandering-braided systems, where bar morphology and reworking drives planform adjustment (Surian et al., 2009). Church and Jones (1982: 292) proposed that “description of these features and consideration of their origin is tantamount to describing the form and enquiring into the stability of the entire river channel”. However, despite their importance, the challenges associated with capturing precise and spatially continuous grain-size data across bar surfaces has provided a major limitation to modelling sediment entrainment and, as a result, bar reworking (Verdú et al., 2005).

The primary, traditional approach to analysing bar sedimentology relies on physical measurements of grain-size through Wolman transect counts or sieving (Wolman, 1954, Church and Jones, 1982, Bunte and Abt, 2001, Kondolf et al., 2003, Hoyle et al., 2007, Rice and Church, 2010). These techniques rely on manually measuring grain-size to establish grain-size distributions for a specific unit or bar (Rice and Church, 2010). This limits grain-size comparison to between units or bars, reducing the ability to analyse grain-size distribution within units and across the bar as a whole,

rather than examining within-bar variability. In recent years, remote sensing techniques have been used to derive statistical summaries of grain-size (e.g. D_{16}, D_{50}, D_{84}; the grain-size at which 16, 50 and 84% of b-axes are finer) at patch to catchment scales. Photographic or "photosieving" methods include those that analyse image texture using semivariograms (Carbonneau et al., 2004, Verdú et al., 2005 Black et al., 2014), analyse image intensity by autocorrelation (Rubin, 2004, Barnard et al., 2007), identify individual grains (Graham et al., 2005), and use Fourier-optics principles (Buscombe and Rubin, 2012). Alternative approaches have used high-resolution Digital Elevation Models (DEMs) from Terrestrial Laser Scanning (TLS; Heritage and Milan, 2009, Hodge et al., 2009, Brasington et al., 2012, Baewert et al., 2014, Schneider et al., 2015, Storz-Peretz and Laronne, 2018) and Structure-from-Motion surveys (Westoby et al., 2015, Vázquez-Tarrío et al., 2017, Woodget and Austrums, 2017) to derive relationships between topographic roughness (i.e. the vertical variation in elevation) and grain-size. Pearson et al. (2017) review empirical relationships that have been derived between D_{50} and roughness metrics, presenting a decision tree to aid the selection of appropriate regression relationship depending upon sediment sorting, shape and packing. These remote sensing techniques represent progression towards characterising bar-scale grain-size variation. As yet, however, applications of these techniques have been largely restricted to methodological development rather than providing data to shed light on fluvial morphodynamics.

High-resolution measurement of topography and grain-size variation presents an opportunity to enhance models of sediment entrainment and the reworking of bar surfaces. Previous attempts to measure bar reworking include the use of sediment tracers or painted patches to measure transport on bar units (Laronne and Duncan,

1992, Carling et al., 2006, Surian et al., 2009, Mao and Surian, 2010, Mao et al., 2017,), capture of sediment in traps or pits (Bridge and Gabel, 1992, Habersack et al., 1998), topographic surveys for sediment budgeting (Brasington et al., 2000, Fuller et al., 2003, Williams et al., 2011), installation of scour chains to measure at-a-point scour (Leopold et al., 1964, Rennie and Millar, 2000, Rodrigues et al., 2012) and aerial photography to depict rates of adjustment (Church and Rice, 2009, Rice et al., 2009, Ham and Church, 2012). However, these approaches measure sediment transport as or after it occurs. Models that predict sediment entrainment across bar surfaces are notably absent. In part, this is due to the logistical challenge of directly measuring the spatial distribution of hydraulics and bedload transport during high-flow events in natural gravel-bed river settings (Williams et al., 2015). If high-resolution topographic datasets (Tarolli, 2014, Passalacqua et al., 2015) are available, two-dimensional flow modelling (e.g. Pasternack et al., 2006, Hodge et al., 2013, Williams et al., 2013) can be used to predict spatial distributions of depth and velocity for particular flow events, thereby enabling bed shear stress to be mapped.

Bar reworking is a key measure of the geomorphic effectiveness of flood events (Wolman and Gerson, 1978). Systematic appraisal of forms and rates of channel adjustment and stability is an important part of river restoration and management applications (Doyle et al., 2007). In such analyses it is important to specify the geomorphic role of flood events of differing magnitude-frequency relations. Bankfull flows are commonly cited as channel forming (formative) events, as flow is concentrated within the banks, before being dissipated on the floodplain at higher flow stages (Leopold et al., 1964, Williams, 1978, Sambrook Smith et al., 2010). It is well established that channel morphology is shaped by multiple discharges. For example, Phillips (2002) found that ‘bi-modal dominant discharges’ shaped channels, whereby

flows below bankfull flush fine sediment and maintain channel shape, whilst rare floods rework coarse sediment and erode channel banks. Surian et al. (2009) found that floods with a discharge of 20% to 50% of bankfull could mobilise the wetted channel, whilst bankfull discharge was necessary to rework higher elevation bar surfaces. This paper provides a quantitative approach to understand the geomorphic effectiveness of these different flows.

Bars are commonly considered to be made up of a resilient, stable 'nucleus' around which more mobile units are deposited on the falling limb of floods (Leopold et al., 1964, Bluck, 1976). This node of coarse sediment indicates flow competence during high magnitude events, whereas the smaller, more active fraction is reworked more frequently. 'Hydraulic' elements, which reflect deformation of the channel bed, can be differentiated from 'storage' elements which store sediments that are being transported through the reach, over variable timeframes (Church and Jones, 1982). Over time, different mechanisms of bar formation determine the range of grain-sizes within a bar. This, in turn, influences the size of event (or events) that is necessary to entrain these different units, reworking and resetting the physical template (dynamic physical habitat mosaic) of the river. Assessing the reworking of barforms within dynamic, multi-channelled gravel-bed rivers is fundamental to understanding channel adjustment at the reach scale. Despite this, previous frameworks which quantitatively assess bar reworking are scarce and predominately limited to tracer studies (c.f. Laronne et al., 2001, Hassan and Ergenzinger, 2005, Carling et al., 2006, Surian et al., 2009). Investigations have traditionally been limited by the difficulties of acquiring grain-size data at an appropriate scale for modelling and characterising reworking (Verdú et al., 2005). Instead bedload transport equations (and associated modelling) usually use single grain-size distributions to represent entire bar surfaces, and, as

such, incorporate a high degree of error (Ferguson and Ashworth, 1992, Hicks and Gomez, 2003, Wilcock et al., 2009, Gray et al., 2010).

Efforts to improve quantitative assessment of the sediment regime of a river (sensu Wohl et al., 2015) depend upon reliable measurement of bed material movement over differing surfaces along a river course at different flow stages. To date, systematic appraisal of grainsize variability has limited the capacity to conduct such modelling exercises. This study analyses these relationships for a dynamic gravel bed river on the North Island of New Zealand. It investigates how patterns of bar reworking are controlled by bar unit scale variations in morphology and sedimentology, reach-scale controls, and flood magnitude. Using data acquired along a wandering-braided reach of the Tongariro River, New Zealand, the objectives of this paper are to: (i) analyse historic bar reworking; (ii) map hyperscale bar topography and grain-size; (iii) develop a novel modelling approach which calculates sediment entrainment and bar reworking across a range of flood magnitudes, using predicted bed shear stresses from two-dimensional hydraulic modelling. This approach offers insight into wider geomorphic questions including: (i) how do mechanisms of bar formation determine bar sedimentology?; (ii) how do reach-scale controls (slope, valley confinement) alter patterns and rates of bar reworking?; and (iii) which flood events are geomorphologically effective in reworking bars in different reach settings?

2. Study Area

2.1. Catchment Description

The Tongariro Catchment (777 km^2) is located in the central North Island of New Zealand (Figure 1). Catchment elevation ranges from 2797 m above sea level (asl; New Zealand Geodetic Datum 2000) at the peak of Mt Ruapehu to 329 m asl where the Tongariro River drains into the caldera of Lake Taupo (surface area 616 km^2). The

alpine climate in the headwaters grades to more temperate conditions at lower elevations. Mean annual rainfall ranges from 3400 mm at high elevations to 1200 mm at Turangi (Genesis Energy, 2000). Mean total monthly rainfall at Turangi is lowest in February (109 mm) and peaks in July (180 mm). Mean monthly temperatures in the lower catchment range from 6.5^{o} C in July to 17.3^{o} C in February with the yearly average being 11.8^{o} C (NIWA, 2009). Two dams in the upper section of the catchment have decreased mean annual discharge at Turangi from 53 m^3s^{-1} to 29 m^3s^{-1} (Genesis Energy, 2000). As the control gates are opened once flow exceeds 150 m^3s^{-1}, there has been negligible long-term disruption to the flow and sediment regime of the system (Reid et al., 2013). The study reach lies approximately 10 km downstream of the lower dam. The dams have induced little or no change to the frequency and magnitude of flood events > 150 m^3s^{-1} (Reid and Brierley, 2015).

Tongariro National Park comprises the western headwaters of the catchment (Figure 1, zone 1a and 1b). The active volcanic field is underlain by andesitic material. The last significant phreatomagmatic and magmatic event on Mt Ruapehu occurred in 1995-1996 (Nakagawa et al., 1999), although there was a minor phreatic event in 2007 (Kilgour et al., 2010). The neighbouring Mt Tongariro had an avalanche-driven phreatic eruption in 2012 (Jolly et al., 2014). The steep higher altitude slopes provide an unstable and harsh environment that is unable to sustain vegetation other than mosses. However, vegetation on the flatter, lower-altitude central plateau comprises a wide range of alpine desert fauna. This low gradient unit buffers the transfer of sediment from the productive volcanic cones to the Tongariro River channel (Fryirs et al., 2007). The eastern headwaters comprise the Kaimanawa Ranges (Figure 1, zone 2), which are composed of uplifting Torlesse greywacke (GNS, 2009). The Kaimanawa Regional Forest Park is made up of native Beech and Podocarp forest. The upper mid-

catchment (Figure 1, zone 3), of which three of the bars analysed within this study are located, is underlain by sediment deposited by lahars that range in age from 14.7k BP to recent events (Cronin et al., 1997). These deposits are superimposed by pumiceous pyroclastic debris ~ 10 m thick, generated by the Taupo Eruption in 186 AD (Wilson et al., 1980). Land use in this lower section of the catchment is more developed, with plantations of *Pinus Radiata*, low density sheep farming and the town of Turangi (population 2952). The delta region (Figure 1, zone 4) has one of the largest freshwater wetlands remaining in New Zealand (Chagué-Goff and Rosen, 2001).

2.2 Study Reach

The study reach includes four bars within a 10 km reach of predominantly wandering gravel-bed river, with a localised braided section at the downstream extent of the catchment, immediately upstream of the delta (Figure 1; Figure 2; Reid and Brierley, 2015). The upstream three bars, Blue, Red Hut and Breakfast bars, are located within a wandering gravel-bed river that is partly confined by terraces formed by incision into lahar deposits following the rhyolitic eruption of Lake Taupo 1.8 ka BP (sensu Fryirs et al., 2015). The most downstream study bar, Bain bar, is located at the downstream point of a semi-braided section, immediately downstream of terraces, where the valley becomes unconfined causing sediment deposition. Sites were selected to represent downstream decreases in grain-size and slope and differences in valley confinement (see Table 1). Each of these lateral, compound bars are located at points where there was one dominant channel and within a relatively straight section (sinuosity < 1.07) to make them more comparable. Bar type was selected based on being the dominant type within the system. Bar morphology has been shaped by both depositional and erosional processes and events, creating diverse, complex features (Bridge, 2003, Rice et al., 2009, i.e. see Figures 3 and 4).

Hyper-concentrated lahar flows have delivered large volumes of coarse sediment into the lower catchment, exerting a significant influence upon bar planform and sediment characteristics in the study reach (Cronin et al., 1997, Fagents and Baloga, 2005). As a result of terrace incision, lag deposits which line the contemporary channel within the study reach are notably coarser than sediments that are delivered from upstream sources. Sampling undertaken for this study revealed a median grain-size of 289 mm for the terrace face adjacent to Blue bar, compared with median grain sizes of the coarsest locale of the bars of 60-65 mm in the highly sediment-laden tributaries in the Kaimanawa Ranges and 90-170 mm for bars in the less sediment loaded streams that drain the volcanic plateau.

3. Methods

3.1 Analysis of historic bar evolution

Aerial photographs from 1941, 1958, 1964, 1973, 1984, 1993 and 2007, and a survey map from 1928, were digitised to assess the historic evolution of each bar. Analysis of more than 50 years of flood history at Turangi gauging station focussed upon the frequency and magnitude of floods > 400 m^3s^{-1}, capturing all floods greater than the mean annual flood event (which is 480 m^3s^{-1}). This historical record was used to assess the mechanisms of bar development, and to ground analyses of bar reworking and the geomorphic effectiveness of the events.

3.2 Mapping bar surface sedimentology

Each bar was surveyed using a Leica ScanStation 2000 TLS to map bar morphology and surface roughness. Scan stations positioned at multiple locations close to the perimeter of each bar were configured to ensure considerable overlap between adjacent point clouds, thus maximising line of sight and reducing the effect of larger

clasts that create shadow areas in their lee. This configuration required between 7 and 11 TLS scans per bar. A Trimble RTK-GNSS R8 was used to establish a benchmark on each bar. This was then positioned using RINEX data from the nearest static GNSS station in the New Zealand PositionNZ network. A Sokia SET530R Total Station was used to survey scanner and target positions.

Scan data from each bar were georeferenced into a single point cloud using Leica Cyclone software. Point clouds for each bar had between 7 and 17 million points. Each point cloud was manually edited to remove vegetation and delineate the bar margin. Point cloud data were subsequently unified to a quasi-regular 0.05 m resolution, preserving the original positions of selected points, and processed using ToPCAT software (Brasington et al., 2012). This tool processes high resolution, large point clouds to produce statistics at a specified spatial resolution. Topography was mapped at 1 m^2 resolution, using minimum elevation values for each grid cell. The detrended standard deviation, σ_z, was calculated for 1 m^2 patches, thereby removing the influence of slope on local point cloud standard deviation. This was used to map surface roughness across bar surfaces at 1 m horizontal resolution.

A dataset of 27 surface grid-by-number b-axis counts was derived to correlate surface roughness to median grain size. A sample spacing of two times the largest clast was maintained for each sample. Each count consisted of 100 clast samples, except for four small units on Red Hut bar where only 50 grains could be measured to maintain independence (Wolman, 1954, Church and Kellerhals, 1978, Brierley and Fryirs, 2005,). Transects were positioned using Trimble RTK-GNSS. The linear relationship between median grain-size (D_{50}) and mean σ_z yielded an R^2 value of 0.92 (Figure 5), similarly strong as relationships reported elsewhere, which are typically characterised by R^2 c.0.9 (Pearson et al., 2017). In Pearson et al.'s (2017) compilation of

relationships between D_{50} and σ_z (where $R^2 > 0.49$) that have been reported in eight studies, only 4 out of a total of 97 samples were for $\sigma_z > 0.04$ m, with a maximum value of 0.06 m. The Tongariro counts include 11 samples with $\sigma_z > 0.04$ and extends the range to 0.08 m (i.e. the relationship derived here extends the range of grain size previously modelled). The linear relationship derived from the Tongariro counts was used to map median grain-size for each bar from maps of σ_z. Together with DEMs, these maps provided the basis to map geomorphic units across each bar, from which analyses of sediment entrainment and bar reworking were conducted.

3.3 Geomorphic units mapping

Each bar was classified into geomorphic units, characterized as areas with distinct morphological and sedimentological features that are products of particular sets of erosional and/or depositional processes (see Leopold et al., 1964, Church and Jones, 1982, Bluck, 1987, Brierley and Fryirs, 2005, Rice and Church, 2010, Wheaton et al., 2015; Table 3; Figure 4). RTK-GNSS was used to map these units. ArcGIS was used to differentiate units based on topography and grain-size data from the TLS scans.

3.4 Modelling steady state flow

Reach-scale hydraulic models were used to predict depth and velocity patterns across each bar, for flood flow scenarios with recurrence intervals (RI) of 2.33 ('mean annual flood'), 10, 20, 50 and 100 years. Discharges for each event were derived using a Gumbel Type 1 Extreme Value distribution from 50 years' of discharge data from the Tongariro River at Turangi gauge (Table 2). These flood events are referred to within this paper as Q2.33 – Q100.

The hydraulic modelling software package, JFlow® (Crossley et al., 2010), was used to perform hydrodynamic calculations. JFlow® solves the two-dimensional depth-

averaged shallow water equations and has been demonstrated as suitable for flood risk modelling over a wide range of conditions in benchmark tests published by the official flood management authority in England (Environment Agency, 2013). The numerical solver is a Godunov-type finite volume implementation of Roe's scheme (Roe and Pike, 1984, Toro, 2001) that is well-balanced, shock-capturing and includes treatment of wetting and drying of cells. It is therefore capable of resolving the spatial and temporal evolution of flow depths and (depth-averaged) velocities in a flood wave advancing over complex topography that may induce both sub- and super-critical flows. Each of the five flood flow scenarios was simulated by increasing the applied discharge gradually to the specified peak flow and holding the flow at that rate until steady-state flood depths and extents were produced. Bed shear stress was calculated using predicted depths and velocities (see equations 1 and 2, below).

A JFlow® model was built for each bar, with a regular 1 m horizontal resolution grid. The longitudinal spatial extents of each model domain varied from 1.2 to 2.1 km (Figure 2). Model topography was generated by fusing together three sources of distributed elevation data. First, the topography of each bar was represented using the TLS survey data. Second, 1 m resolution airborne LiDAR, acquired by New Zealand Aerial Mapping Limited on 19 June to 24 July 2006 was used to represent topography that was greater in elevation than the river water surface. Third, optical-empirical bathymetric mapping techniques (Legleiter et al., 2004, Feurer et al., 2008, Williams et al., 2014) were used to derive channel bathymetry using 0.6 m resolution RGB imagery that was acquired concurrently with airborne LiDAR. Depth data were acquired from a longitudinal echosounder survey undertaken using a Sonarmite Transducer and Trimble Nomad GPS on 12 February 2010. This survey was undertaken at a similar flow stage to those when the aerial imagery was acquired.

There were no geomorphologically effective flow events between the time of aerial imagery acquisition and the depth survey. Various optimal-empirical linear transform and band ratio models were tested, using data (n = 1749, mean observed depth = 1.14 m) that cover the spatial extent of the hydraulic model domains. A linear transform method (Lyzenga, 1981) using the red spectral band performed best and achieved a depth Root Mean Square Error (RMSE) of 0.62 m. Whilst this RMSE is higher than typical vertical errors associated with the airborne LiDAR data component of the DEM, it was deemed acceptable for the purposes of providing bathymetry for reach-scale bathymetric modelling at high flows.

Model roughness was set to a constant Manning's 'n' value of 0.03. This was based on extending the relationship between Manning's 'n' and discharge for the Tongariro at the Turangi gauge (Hicks and Mason, 1991) to account for decreased influence of bed roughness on flow during high magnitude events. Sensitivity tests were performed to ensure that the downstream boundary of each model was positioned sufficiently far downstream so as not to influence flow predictions across each bar. Hydraulic predictions were verified using a spatially dense set of acoustic Doppler current profiler (aDcp) measurements that were acquired across a confluence unit within the Bain bar model domain. A Sontek M9 RiverSurveyor aDcp was mounted on a trimaran, positioned using RTK-GPS and moved across the channels in zig-zag transects using tethers, thus using the same field procedures as those described by Williams et al. (2013; 2015). The total longitudinal length of the survey was 215 m. For the verification simulation, model bathymetry within the aDcp survey extent was based upon the aDcp bed level measurements. Discharge was estimated at the upstream boundary of each of the two channels that met at the confluence by sampling transects from aDcp data that had been spatially interpolated using ordinary kriging. Kriging was undertaken

using the same procedures as those described by Rennie and Church (2010). A total of 6,470 aDcp depth and velocity measurements were compared to model predictions. Results are shown in Table 4. Overall, the errors are acceptable. The negative bias in the depth mean error (-0.045 m) is likely caused by uncertainty in the flow input and distribution at the model upstream boundary and topographic uncertainty since the aDcp bathymetry was fused into the DEM that was built from airborne LiDAR and optical-empirical bathymetric mapping. The magnitude of other error statistics are similar to those reported by Williams et al. (2013) using Delft3D for shallow water predictions in the braided Rees River.

3.5 Modelling sediment entrainment and bar reworking

The maps of median grain-size were used to model sediment entrainment and bar reworking for flood events associated with different magnitude-frequency flow events. This was achieved by calculating the erodibility ratio, E, of dimensionless shear stress, τ, (impelling forces) to critical shear stress, τ_c, (resisting forces) thus using the Shields equation for sediment particle entrainment (Shields, 1936, Chanson, 2004, Church, 2010):

$$E = \frac{\tau}{\tau_c} \quad (1)$$

Bar reworking was calculated for each of the five flood events to measure geomorphic effectiveness. Bed shear stress was calculated as

$$\tau = \frac{g\rho u^2}{C^2} \quad (2)$$

where u is modelled depth-averaged velocity, ρ is water density and C is the Chezy coefficient which was calculated from modelled depth, h, and the Nikuradse roughness length, k_s:

$$C = 18^{10}\log\left(\frac{12h}{k_s}\right) \quad (3)$$

k_S is commonly expected to take a factor, α_x of a representative particle size, *d*:

$$k_s = \alpha_x d_x \quad (4)$$

Here, d_x is taken to be the median grain-size, D_{50} (as mapped in Figure 4) estimated using the relationship between D_{50} and σ_z (Figure 5). The scaling factor, α_x was taken to be 1 based on the values of Keulegan (1938) and Meyer-Peter and Muller (1948).

To calculate the threshold of motion for particles, an equation for critical shear stress, τ_c, was obtained by equating the shear force acting to overturn a particle and the submerged weight of the particle:

$$r_c = \theta_c g d(\rho_s - \rho) \quad (5)$$

where θ_c is the dimensionless critical shear stress, *g* is acceleration due to gravity, *d* is a representative particle size, and ρ_s is particle density. Since the focus of this paper is upon characterising bar surface sedimentology using the median grain-size, *d* was assumed to equal D_{50}. The four bars considered are composed of a mix of andesite (ρ_s = 2565 kg m^{-3}; (Tenzer et al., 2011)) and greywacke (ρ_s = 2639 kg m^{-3}). Since ρ_s are similar for these two mineralogies, the mean ρ_s of 2602 kg m^{-3} was used.

Soulsby and Whitehouse's (1997; in Coleman and Smart, 2011) curve fit of the Shields curve was used to calculate θ_c:

$$\theta_c = \left[\frac{0.30}{1+1.2D_*}\right] + 0.055\left[1-\exp(-0.020D_*)\right] \quad (6)$$

The dimensionless grain-size, D_*, was calculated from:

$$D_* = \left[\frac{g(s-1)}{v^2}\right]^{1/3} d \quad (7)$$

Where g is gravitational acceleration, s is specific gravity of the sediment, v is kinematic viscosity at a specific water temperature and d is grain-size in m, for which the 1 m^2 resolution raster grid of median grain-size (D_{50}) was used. The mean temperature in the Tongariro, 10 °C, was used to yield a viscosity of 1.267×10^{-6} $m^2 s^{-1}$. Wilcock (1992) suggests that a fit of the Shields curve (equation 6) can be used for a gravel mixture to estimate τ_c for a gravel mixture. Furthermore, equal mobility suggests that in a mixture all grain-sizes are entrained at about the same shear stress due to particle hiding and protrusion effects. Here, θ_c is calculated at a 1 m^2 resolution to reflect the spatial variation in D_{50} across each bar. Since the analysis of reworking is aggregated to the scale of individual bar units (Figure 4), it is assumed that spatial variation in D_{50} is the primary cause of variation in entrainment across each bar unit.

Finally, the measure of relative erodibility (equation 1) was calculated by dividing bed shear stress (equation 2) by critical shear stress (equation 5). This measure does not attempt to account for the inherent complexities of sediment transport, including turbulence and non-uniformity of flow such as eddies. However, the approach is designed as a simple and accessible framework to investigate the susceptibility of different geomorphic units to sediment entrainment, and to characterise and compare patterns of bar reworking. In this context, “accessible” refers to the availability and relative ease and speed of application of a model such as JFlow®, which nevertheless offers a robust physical basis for depth and velocity simulation of flood flows. The approach also offers a potential pathway to develop a more detailed modelling scheme

in future, predicated on continuing improvements in computer processing power and monitoring technology. For example, a numerical scheme of the same type as the JFlow® code used here has been extended by Guan et al., (2016) to include a non-equilibrium sediment transport model and corrections for secondary (helical) flows around channel bends, and shown to be capable of simulating morphological changes in laboratory and field scale experiments. However, the inclusion of sediment dynamics and a secondary flow correction involves significant computational cost, and is beyond the current state of art in models applied routinely in geomorphological management practice. Here, a pragmatic approach is taken utilising a related class of hydrodynamic model (JFlow®) to predict flow depth and velocity fields under a range of scenarios, from which inferences may be made about morphological change, albeit subject to some approximation. The JFlow® code is particularly useful in this context because it was written to target high-performance GPU (Graphics Processing Unit) parallel processing, which means simulations can be run quickly without the need for dedicated High Performance Computing facilities.

4. Results

4.1. Bar evolution and historical adjustment

To set the context for analysis of sediment entrainment of each of the study bars, the history of bar formation and adjustment is first related to the history of high magnitude flood events (>400 m^3s^{-1}; Figures 3 and 6).

4.1.1. Blue bar evolution

A bar has existed at this location since 1958, giving the bar an age of over 50 years (Figure 3). The bar was most likely created or reworked by the Q60 flood in 1958, directly before the aerial photograph was taken (Figure 6). The Q20 flood in 1964

stripped the bar of vegetation. Bar size and vegetation cover at a given time reflects the period elapsed since the last large magnitude flood event (> Q20). For example, revegetation and incorporation of the bar into floodplain between 1973 and 1993 coincided with a period of few flood events, all of which were smaller than Q10 (Figure 6). The Q60 flood in 2004 stripped the bar of vegetation and reworked the bar surface resulting in the reappearance of an unvegetated bar in the 2007 survey. In summary, Blue bar appears as a small, relatively homogeneous bar (compared with the others in this study) which has undergone little morphological adjustment and requires flood events > Q20 to strip and mobilise the surface.

4.1.2. Red Hut bar evolution

Red Hut bar has a complex history with evidence of significant adjustment to barforms following floods, and little change in-between these high flow events (Figure 4). The head and much of the supra-platform of the contemporary lateral bar was present in the survey map from 1928. Indeed, a proportion of the head and supra-platform of the bar were present in the same location throughout the series of aerial photographs. Between 1928 and 1958, likely following the 1958 flood (< 100-year flood recurrence), a back channel formed and Red Hut bar became a mid-channel bar. By 1964, the mid-channel island overlapped with the current bar head and supra platform, and the back channel was narrower. By 1973 a lobe of sediment had been deposited in the lee of the upstream Poutu Island, connecting the two. The bar outline at this point comprised most of the current bar head and supra-platform, and it remained like this through the 1984 and 1993 surveys, with a small back channel present. In 2004, a Q60 flood stripped vegetation and the bar once again became a mid-channel feature, as seen in the 2007 map, similar to the response following the 1958 flood. Google Earth imagery from 2015 shows that the bar had formed its contemporary shape as a lateral bar,

giving its current shape an age of between 3 - 4 years. This history describes a consistent response following large floods from a lateral to a mid-channel bar, and then reverting back to a lateral bar between these events. There are two scenarios for this adjustment: (i) the mid-channel bar is formed by reworking of sediments on the preceding bar; or (ii) that mid-channel bar is formed by deposition of sediment delivered from upstream by the large flood.

4.1.3. Breakfast bar evolution

Breakfast bar has been relatively stable since 1958 undergoing minimal adjustment in the past 80 years (Figure 4). This bar exhibited similar patterns of adjustment to Blue bar. Vegetation cover increased and the bar was integrated into the floodplain between 1973 and 1993 as few flood events occurred. The 2004 Q60 flood again stripped vegetation. Thus, Breakfast bar has an age of > 50 years and has undergone minimal adjustment. Large magnitude flood events (> Q20) are required to remove vegetation, and rework and deliver sediment.

4.1.4. Bain bar evolution

Bain bar is located downstream of the terrace-constrained reach. This semi-braided section of river drains an actively reworked alluvial fan. Channel widening between 1958 - 1964 reworked the surface of the dynamically adjusting braidplain within which the contemporary bar has formed (Figure 3). Gravel extraction in 1973 caused artificial narrowing (Reid and Brierley, 2015). The channel adopted a low sinuosity, single channel planform with fewer active bar surfaces. Between 1973 and 2007 this reach widened, increasing the area of actively reworked bar surfaces. A bar surface was first observed at the bar's present location in 1993, giving the bar an age of > 18 years (i.e. this bar is a relatively young and dynamic feature).

4.2. Relative erodibility as a measure of bar reworking

Within-bar geomorphic units were used to identify areas and predicted rates of reworking. Figure 4 presents maps of grain-size across each bar, annotated with geomorphic unit outlines. Maps of modelled bar reworking are shown in Figures 7 and 8. The distribution of patches that are predicted to undergo sediment entrainment across the range of modelled flood events is indicated. The percentage of each geomorphic unit predicted to be entrained during each modelled flood event is summarized in Table 5. Note, the percentage of bar reworking in the following section refers to predictions of the model based on the current channel morphodynamics.

4.2.1. Spatial distribution of bar reworking

The highest proportion of reworking during the Q2.33 event for the study bars was demonstrated at Blue Bar (33%). 74% of the bar tail is entrained during this flood, including the coarse gravel to sand fractions that make up the tail, and coarse cobble on the channel margins (Figure 7; Table 5). During the Q10 flood, cobble to coarse cobble in the back channel (59%) and the supra-platform (83%) is entrained, indicating significant bar reworking. Larger floods are needed to mobilise the boulder-sized grains on the bar head, with entrainment increasing from 10% to 43% at the Q10 flood, then up to 63%, 81% and 97% for the Q20, Q50 and Q100 floods respectively. Overall entrainment for Blue bar is high for the larger floods, with 91% and 97% of the bar entrained during the Q50 and Q100 floods.

During the Q2.33 flood, gravel to sand sized sediment located on the bar tail (68% entrained) and upstream supra-platform (37%) of Red Hut bar is entrained (Figure 7; Table 5), but the rest of the bar remains largely static (< 21% entrainment). The Q10 flood causes a 4% increase in the reworking of the total bar, which increases from 26% during the Q2.33 flood to 30%. This is primarily due to a slight increase in

reworking of the supra-platform (39% entrainment on the upstream supra-platform and 14% on the downstream supra-platform), which make up 56% of the bar surface. Minimal increases in reworking are seen for large flood events, with the overall bar reworking increasing to 31%, 33% and 34% for the Q20, Q50 and Q100 floods respectively. This bar undergoes the lowest degree of reworking of the study bars. A high elevation ridge of large sediment (coarse cobble to boulder) runs along the middle to top of the bar head. Increases in flood magnitude do not change the proportion of this geomorphic unit that is entrained, with a consistent percentage entrainment of 21% across all flood events. This indicates the inherent stability of this bar. However, Red Hut was the youngest of the bars, an apparent contradiction which is discussed in Section 5.1.

During the Q2.33 flood, the majority of the fine gravel and sand is entrained from the tail (81% entrainment) of Breakfast bar (Figure 8; Table 5). The Q10 flood mobilises a greater area of cobbles from the supra-platform than the Q2.33 flood, with an increase from 6% to 36% for this unit. The moderate elevation head is comprised of relatively coarse material (predominately coarse cobble) which runs along the upper-middle section of the bar adjacent to the channel. A lesser proportion of the head is likely to be reworked compared with the tail, and a greater proportion of the head is likely to be reworked relative to the supraplatform. This bar has a relatively high entrainment at the Q100 of 86% despite being one of the oldest bars. This reach is constrained between stopbanks and the terrace, which results in the high energy and level of entrainment, but also restricts planform adjustment. This means that sediment may be eroded to this location, but it also gets recurrently deposited here as this left bank location is more protected than the right.

Smaller grains on the back channel (41%), tail (11%) and supra-platform (13%) are entrained during the Q2.33 flood on Bain bar (Figure 8; Table 5). Cobbles that primarily make up the bar head are less likely to be reworked (3%). The Q10 flood increases entrainment in the supraplatform from 13% during the Q2.33 to 35%. As flows increase to the Q100 flood, the proportion of each geomorphic unit that is entrained only increases by 1% to 5%. For the Q100 event, 35% of the total area is predicted to be reworked, partly due to the stability of the bar head, where only 13% of it will be reworked.

4.2.2. Patterns of total bar reworking

Figure 9 displays the percentage of each bar entrained across the range of flood events. This allows variation in reworking to be assessed. Blue and Breakfast bars have similar trends in reworking, but reworking is more recurrent on the former. As flood magnitude increases from Q2.33 to Q10, the proportion of the bar tail that is reworked increases to >90%. Overall bar working between these two flood events increases from 33% to 64% for Blue bar, and 26% to 52% for Breakfast bar. For larger flood events there are consistent increases in reworking across the head and supra-platform units for both bars, and across the back channel unit for Blue bar.

Compared to Blue and Breakfast bars, Red Hut and Bain bars have much lower proportions of reworking across all flood events. Red Hut bar shows a gradual increase in total reworking as discharge increases, from 26% for the Q2.33 event to 34% for the Q100 event. Bain bar shows a greater increase than Red Hut bar between the Q2.33 to Q10 event (15% to 33%) but subsequent increases in discharge show relatively little change in the area of reworking with the Q100 event, with a percentage entrainment of 35%.

5. Discussion

5.1. Mechanisms of bar development

Hydraulic modelling of sediment entrainment conducted using hyperscale resolution mapping of bar sedimentology, interpreted in relation to longer-term (multi-decadal) analysis of geomorphic adjustments, provides key insights into the geomorphological effectiveness of differing flood flows and their capacity to rework bars along the lower Tongariro River. Using the terminology proposed by Church and Jones (1982), the study bars are comprised of a combination of hydraulic and storage elements, with significant differences in the likelihood of reworking of Blue and Breakfast bars (primarily made up of hydraulic elements) relative to Red Hut and Bain bars (primarily made up of storage elements).

Blue and Breakfast bars, which are located at the upper and lower sections within the terraces, were formed by large floods (> Q50) which stripped vegetation and fine-grained sediment from the floodplain, uncovering a lag of coarse boulder material that formed the bar head. As such, the bulk of each bar is a hydraulic element. This was reflected in a high proportion of the bar area (40-41% of the bar area compared with < 33% for the other bars) which was classified as bar head and characterised by coarse cobble. Despite having a larger coarse node, these bar heads underwent increased reworking for each larger flood event. By contrast, bar tails underwent no or minimal increase in the degree of entrainment for any flood larger than the Q10. Little or no evidence of systematic increase in size and linear growth further supports the characterisation of these bars as hydraulic elements, as storage elements would be expected to undergo changes to their shape, reflecting changes to sediment supply from upstream (Bridge, 2003, Church and Rice, 2009). By contrast, bar size reflected

time elapsed since the last flood event large enough to rework the bar and floodplain surface, stripping vegetation (> Q20).

Red Hut has a more complex evolutionary history. A mid-channel bar formed following floods which reverted back to a lateral bar over time. This morphology has been maintained in the period between major floods over the last 90 years. Modelling analysis identified that despite the terraces being wide at this point, there is a localised bedrock pinch which creates a much narrower hydrological valley width. This caused a backwater effect which encourages deposition at this location and minimised kinetic flow energy such that only 34% of the surface area could be entrained by the Q100 flood. Based on this analysis, the lateral bar that was present at the time of survey, and also appears on the 1928 map, can be considered to represent a relatively static hydraulic element. In contrast, the mid-channel bar that appears post-flood is likely to be a storage element, and a function of the increase in sediment supply during very large flood events, which then stalls at this location, superimposing this bar over the underlying lateral bar. This also highlights the stability of the bar head and the supra-platform in location. Ashworth (1996) presents a model for mid-channel bar growth, where sediment is deposited downstream of a confluence, where flow converges causing scour and then diverges causing deposition. Similar processes may have caused the deposition of the coarse nucleus of Red Hut bar, as flow converges downstream of Poutu Island, which has existed since at least 1928. This Island acts to protect the area within which Red Hut bar is located, allowing storage of the finer fraction. In comparison, the finer material at the tail of the bar was far more transient (c.f. Church and Rice, 2009), and back channels were able to form on the edge of the current bar location.

The whole of Bain Pool, the farthest downstream bar in this study, can be classified as a storage element. The floodplain-delta was formed following the Taupo eruption, 1.8 ka BP (Wilson and Walker, 1985, Smart, 1999, Rosen et al., 2002) and, as such, consists of sediment which is delivered by the contemporary regime. The bar reworking mapping supports this bar as a storage element since sediment on the head and supraplatform, and a significant portion of the tail, are shown to be resilient to entrainment during all the flows simulated. In this semi-braided reach, bar adjustment is likely a consequence of bank erosion (Wheaton et al., 2013) altering bar morphology, as shown from the historic record of frequency bar reworking. Thus, at this location, rather than the most common model of initial bar development which is the formation of a unit bar head and then the deposition of additional secondary units (Ashmore, 1982, Ashworth, 1996, Bridge , 2003, Lunt and Bridge, 2004, Church and Rice, 2009), bar reworking is a function of the switching, lateral migration and alignment of primary channels.

Models of mid-channel bar development describe coarse sediment being deposited at a locale of decreased shear stress, facilitating further deposition of smaller material downstream (Ashmore, 1982, Ashmore, 1991, Ashworth, 1996, Knighton, 1998, Bridge, 2003). However, for the terrace-confined bars within the Tongariro River, the active fraction delivered from upstream is combined with the lag of lahar boulders which is reworked to form bar heads. As such, bar development is not simply a function of decreases in shear stress capturing mobile fractions, but also the moulding and redistribution of this larger fraction which may be retained within the reach across long residence times (100-1000 years). This makes the role of ‘hydraulic elements’ in bar formation especially pertinent within this system. Most existing models of bar development are created for rivers with active beds, especially within flume work

(Ashmore, 1982, Ashmore, 1991, Ashworth, 1996, Knighton, 1998, Bridge, 2003,) although recent experiments have begun to consider the role of coarse sediment (MacKenzie and Eaton, 2017). This highlights the need to further investigate the influence of lag sediment (volcanic, glacial or due to decreased stream capacity following regulation) from other sedimentary influences on bar development and channel adjustment across a range of rivers. Hence, assessing the landscape memory and the resulting calibre and volume of legacy sediments can be crucial for understanding the sensitivity of the system.

5.2. Influence of reach position on bar reworking

The data assembled for this study indicate that reach-scale controls, such as slope and valley confinement, alter patterns of reworking. The Q2.33 flood entrained a lower proportion of Bain bar (15%) than the three other bars (26-33%). For floods > Q2.33, the extent of reworking is greater for Blue and Breakfast bars than Bain and Red Hut bars. As Blue and Breakfast bars are both in terrace-confined valley settings, they are subjected to higher flow velocities than the other two bars. Red Hut bar is located immediately upstream of a bedrock-controlled valley pinch point, despite wide terrace-width at this point. This pinch point causes a backwater effect during high flows which reduces flow velocity. As Bain bar is located in an unconfined reach, increases in flow are accommodated by flow expansion across the floodplain, in a similar fashion to that described by Magilligan (1992). As Blue Bar has a steeper slope than Breakfast bar, flow is characterised by higher kinetic energy (Table 1). Across all the flood events a greater proportion of Blue bar is worked compared to Breakfast bar, although the trends in reworking are similar between the bars (Figure 9).

Bain bar is located within the braided reach on a depositional floodplain. Remnant or reworked lahar deposits are not evident in this reach, so the grain-size distribution is

more strongly influenced by sediment delivered by the contemporary regime (Reid and Brierley, 2015). The low percentage of bar reworking that is predicted for Bain bar is consistent with this bar being a storage element. The marked decrease in slope along this reach is reflected in the gravel-sand transition immediately downstream of Bain bar. As such, this zone traps larger cobble-sized sediment which the channel is not competent to transport further downstream.

5.3. Conceptual model of geomorphic effectiveness of floods

Geomorphic effectiveness represents an on-going theme of study within geomorphology, as it recognises the importance of different flood magnitudes in channel evolution (Costa and O'Connor, 1995). Usually geomorphic effectiveness is related to maintenance of the channel shape or cross-section, with effectiveness measured as the volume of sediment transported for different sized floods (Wolman and Gerson, 1978, Andrews, 1980, Lenzi et al., 2006). More recent approaches have started to relate sediment transport on gravel bars to geomorphically-effective flows (e.g. Surian et al., 2009). However, these studies are spatially and temporally limited since they consider geographically discrete patches upon a bar. In addition, analysis is dependent upon the magnitude of flood events which occur during a sampling period, which may not capture the system's morphologically formative events. Thus, the bar reworking approach developed within this paper allows for geomorphic effectiveness to consider the whole of the bar and the range of flood events perceived to be effective at reworking this system.

Figure 10 presents a conceptual model that classifies the proportion of each bar unit that is reworked by different magnitude flood events based upon valley confinement. For bars in confined locations, the Q2.33 flood flushed fine grained material from the tail of all bars (40-70%), as well as mobilising 30% of the supra-platform and back

channel for bars in settings with a constant valley width. The Q10 flood greatly increased entrainment of material in terrace-confined bars with constant valley width but caused only a slight increase in sediment mobilisation for the bar in a terrace-confined setting where the valley width narrowed due to a local bedrock pinch point. This is due to comparatively lower bed shear stresses over the bar than in a constant valley width setting because the valley pinch-point causes a reach-scale backwater effect, reducing flow velocity. The pattern of changes in bar reworking was similar at these confined settings for flow increases between Q10 and Q50, and Q50 and Q100. The bar in an unconfined setting shows much lower rates of bar reworking than for the bars in confined settings. Moreover, increases in reworking are relatively limited as flow is increased. This is because increases in flow are accommodated by increases in the wetted width of the floodplain, with only slight increases in depth and velocity across the bar.

The evidence collated in this paper suggests that a range of discharge magnitudes are necessary to explain the geometry and surface sedimentology of bars. Within the Tongariro, small floods (Q2.33) are most likely to flush and deposit smaller gravel fractions on the tail of bars in confined settings and along the back channel of bars in unconfined settings. These floods are likely responsible for the majority of sediment transport through the reach, especially moving the smaller active material delivered from the eastern sub-catchment that includes the Kaimanawa Ranges. However, these floods have minimal influence on channel change. In contrast, larger floods (> Q20) are required to entrain the coarse cobble-boulder fraction on the supra-platform and head of the bar in confined settings with constant valley width. Whilst these floods may not cumulatively transport as much sediment as the smaller, more frequent events (c.f. Wolman and Miller, 1960) they are far more geomorphically effective at

reworking the lahar boulder lag deposits and eliciting planform change. Bars that are located immediately upstream of valley narrowing are shown to be relatively resilient to bar reworking compared to those located in confined valleys with constant width.

The conceptual model highlights that bar heads are typically the least likely bar unit to be entrained during any given flood event. This similarity occurs despite the marked differences in slope, grain-size and mechanisms of bar adjustment between the reaches. This indicates that the bar head deposit is graded to each reach position to obtain a balance between the coarse fraction and the shear stress generated during these frequent floods. Indeed, Brummer and Montgomery (2006) discuss the role of coarse clasts in providing a 'stable nuclei' for step formation and Carling (2006) suggests that bars act as ramps, which feed finer grained sediment to the body and tail of the bar, providing a rationale for fining. Within the Tongariro system, bar formation requires the deposition or concentration of a nucleus of clasts large enough to be resistant to frequent flood events. These relative 'nodes of stability' then precipitate deposition and protect more transient material to their lee (as suggested by Carling, 2006), creating units shaped by different formative events and, as a result, reworked by different magnitude floods. Whilst it is well documented that bar heads are reworked less frequently than the downstream units (Leopold et al., 1964, Bluck, 1976, Bridge, 2003), understanding which flows bar heads are adjusted to has not been previously documented.

5.4. Evaluation of the bar reworking approach

Recent methodological developments are revolutionising the ability to gain high resolution measures of grain-size, ultimately changing the way that bar geometry and surface sedimentology is quantified. However, to date, most investigations have focused upon the methodological development of these techniques at the 'patch'

scale; few examples exist whereby technology is applied to aid the understanding of geomorphological form and processes at pertinent scales (bar to reach) of enquiry. This paper succeeds in extending the spatial scale of morphological and grain-size mapping using TLS to that of multiple bars and also contextualising contemporary observations with a historical narrative. Moreover, the paper increases the range of grain-sizes previously mapped with this technology to include the cobble and boulder fraction (c.f. Pearson et al., 2017). This was used to offer insights into the mechanisms of bar evolution and provide a foundation upon which bar reworking could be analysed.

A major strength of the bar reworking approach is the ability to calculate sediment entrainment at the scale at which grain-size varies, implicitly allowing questions based on the characteristics of the specific bar to be asked. This highlights that wandering gravel rivers have variable entrainability, and are thus more complex than many of the bar free systems that entrainment theory and analysis was based on (Ashmore, 1982; Bridge 2003). In addition, modelling entrainment for specific flood magnitudes provides benchmarks of adjustment, from which likely future pathways of adjustment can be predicted. This aids determinisation of the likelihood of prospective moving targets for river management (see Brierley and Fryirs, 2016). This recognises that while it is not possible to predict future distributions of flood events, it is possible to predict the likelihood of how a system will respond to flood events of a given size. The aerial photograph and flood analysis provided a historical database with which to compare and explain the predictions made with the model with past patterns of bar response. The bar reworking approach could be extended to evaluate the dynamical physical habitat mosaic of gravel bed rivers, for example by using information on the timeframes of sediment entrainment and periphyton removal events (Hoyle et al., 2017).

One of the strengths of this approach is its simplicity, however, this will inherently also present limitations. The simple modelling does not account for secondary flows which improve predictions of bed deformation (c.f. Guan et al., 2016) and nor is it able to predict wider patterns of adjustment and channel shifting which may ultimately erode the bars. The high resolution survey captures a moment in time and if the channel adjusts, then patterns of shear stress and relative erodibility will vary. For this reason, these predictions need to be treated as indicative of likely adjustment based on current morphology. Multiple surveys over time would illustrate how erodibility changes as the channel morphodynamics do and could help validate the approach within a system.

The phenomenon of event sequencing (Beven, 1981, Marutani et al., 1999) will always limit predictive capabilities in geomorphology. In the Tongariro system vegetation growth and density (and roughness) reflect the time elapsed since the last large flood, which may influence sediment entrainment. However, the large floods modelled within this study are expected to be easily competent to strip vegetation and entrain underlying surfaces. As such, it is recognised that these methods present a simplification of sediment transport compared to the complexities of the real world. For this reason, results should be regarded as indicative of process, rather than definitive, as indeed all models should be. In addition, entrainment should be nested with wholescale channel adjustment, where bar morphodynamics may be a function of lateral adjustment rather than simply patterns of erosion and deposition. Emerging technologies that enable the quantification of form and sedimentology present new opportunities to track change in depositional units, putting classical work (e.g. Bluck, 1976; 1987) into a real time sense of formative flow events, reworking processes and preservation potential. In summary, this work was found to successfully create a novel approach for analysing bar reworking, acting to extend both the type and scale of

approach available to characterise bar reworking and underpin future predictions of channel adjustment.

6. Conclusion

Bars have recently been an understudied feature within river systems, despite their inherent importance as nodes of channel adjustment within gravel-based systems. In part, the intricacy of bar sedimentology has been a major limiting factor in the ability to capture the complexity of these surfaces, and predict how they are likely to evolve into the future. This is especially true of sedimentary complex, bimodal systems, where sediment is delivered from non-hydraulic processes, in this case lahars, requiring more complex patterns of reworking, and a wider range of flood events to be mobilised. This study aims to reiterate sentiments from earlier decades about the importance of understanding bar features as indicative of stability and sediment transport at the reach scale (i.e. Church and Jones, 1982) and advocates for the use of contemporary geomatics and two-dimensional hydraulic modelling technology to advance knowledge into the character and reworking of barforms. This enables an assessment of geomorphological effectiveness at the whole bar scale, across a range of flow events.

This paper successfully extends previous attempts to characterise bar reworking by developing a relatively simple approach, which is transferable to other situations, that couples sedimentology and hydraulic forcing to explain bar morphodynamics. The key findings are (i) multiple bar forming discharges exist within the Tongariro system as shown in both the modelling and the historical analysis. Frequent flood flows rework tail and back channel areas, whilst much larger, less frequent floods are required to mobilise the coarse boulder fraction on the bar head and cause channel change; (ii)

bar heads across all reaches were found to be resilient to the mean annual flood; and (iii) valley confinement exerts a primary influence on patterns of bar reworking which in some situations supresses the size of material that can be entrained, and in others allows incremental increases in reworking as floods increase in magnitude. This work provides a process-based appraisal for predicting future patterns of adjustment. For large, volatile systems where planform change is driven by the reworking of bar deposits, rather than upstream sediment supply, these types of enquiry are fundamental. This work acts to push the boundaries of how bar surfaces are modelled, furthering insights into patterns of reworking.

Acknowledgements

Fieldwork was funded by a University of Auckland Doctoral scholarship awarded to Helen Reid and a University of Auckland Cross Faculty grant. Many thanks go to the Professor Simon Holdaway and Tim Mackrell, Department of Anthropology, University of Auckland, for providing field equipment, software and assistance in the field. Numerical modelling was undertaken whilst Richard Williams undertook a Strategic Insight Programme visit to JBA Trust, funded by the Higher Education Funding Council for Wales.

References

Andrews ED. 1980. Effective and bankfull discharges of streams in the Yampa River basin, Colorado and Wyoming. *Journal of Hydrology* 46: 311-330. DOI: 10.1016/0022-1694(80)90084-0

Ashmore PE. 1982. Laboratory modelling of gravel braided stream morphology. *Earth Surface Processes and Landforms* 7: 201-225. DOI: 10.1002/esp.3290070301

Ashmore PE. 1991. How do gravel-bed rivers braid? *Canadian Journal of Earth Science* 28: 326-341

Ashworth PJ. 1996. Mid-channel bar growth and its relationship to local flow strength and direction. *Earth Surface Processes and Landforms* 21: 103-123. DOI: 10.1002/(sici)1096-9837(199602)21:2<103::aid-esp569>3.0.co;2-o

Baewert H, Bimböse M, Bryk A, Rascher E, Schmidt K-H, Morche D. 2014. Roughness determination of coarse grained alpine river bed surfaces using Terrestrial Laser Scanning data. *Zeitschrift für Geomorphologie, Supplementary Issues* 58: 81-95. DOI: 10.1127/0372-8854/2013/S-00127

Barnard PL, Rubin DM, Harney J, Mustain N. 2007. Field test comparison of an autocorrelation technique for determining grain size using a digital 'beachball' camera versus traditional methods. *Sedimentary Geology* 201: 180-195. DOI: 10.1016/j.sedgeo.2007.05.016

Beven K. 1981. The effect of ordering on the geomorphic effectiveness of hydrologic events. In Davies TRH, Pearce AJ (eds.) *Erosion and Sediment Transport in Pacific Rim Steeplands, IAHS-AISH Publication* 132: 510-526

Black M, Carbonneau P, Church M, and Warburton J. 2013, Mapping sub-pixel fluvial grain sizes with hyperspatial imagery. *Sedimentology* 61: 691-711. DOI: 10.1111/sed.12072.

Bluck BJ. 1976. Sedimentation in some Scottish Rivers of low sinuosity. *Transactions of the Royal Society of Edinburgh* 69: 425-456

Bluck BJ. 1979. Structure of coarse grained braided stream alluvium. *Transactions of the Royal Society of Edinburgh* 70: 181-221

Bluck BJ. 1987. Bed forms and clast size changes in gravel-bed rivers. In Richards KS (ed.) *River Channels: Environment and Process.* Oxford: Blackwell

Brasington J, Rumsby BT, Mcvey RA. 2000. Monitoring and modelling morphological change in a braided gravel-bed river using high resolution GPS-based survey. *Earth Surface Processes and Landforms* 25: 973-990. DOI: 10.1002/1096-9837(200008)25:9<973::AID-ESP111>3.0.CO;2-Y

Brasington J, Vericat D, Rychkov I. 2012. Modelling river bed morphology, roughness and surface sedimentology using high resolution terrestrial laser scanning. *Water Resources Research* 48: W11519. DOI: 10.1029/2012WR012223

Bridge JS, Gabel, SL. 1992. Flow and sediment dynamics in a low sinuosity, braided river: Calamus River, Nebraska Sandhills. *Sedimentology* 39: 125-142. DOI: 10.1111/j.1365-3091.1992.tb01026.x

Bridge JS 2003. *Rivers and floodplains : forms, processes, and sedimentary record,* Malden: Blackwell.

Brierley GJ, Fryirs KA 2005. *Geomorphology and River Management Applications of the River Styles Framework.* Malden: Blackwell Publishing.

Brierley GJ, Fryirs KA. 2016. The Use of Evolutionary Trajectories to Guide 'Moving Targets' in the Management of River Futures. *River Research and Applications* 32: 823-835. DOI: 10.1002/rra.2930

Brummer CJ, Montgomery DR. 2006. Influence of coarse lag formation on the mechanics of sediment pulse dispersion in a mountain stream, Squire Creek,

North Cascades, Washington, United States. *Water Resources Research* 42: W07412. DOI: 10.1029/2005wr004776

Bunte K, Abt SR 2001. *Sampling surface and subsurface particle-size distributions in wadable gravel- and cobble-bed streams for analyses in sediment transport, hydraulics, and streambed monitoring.* General Technical Report RMRS-GTR-74. Fort Collins, Colorado: U.S. Department of Agriculture, Forest Service, Rocky Mountain Research Station.

Buscombe D, Rubin DM. 2012. Advances in the simulation and automated measurement of well-sorted granular material: 2. Direct measures of particle properties. *Journal of Geophysical Research: Earth Surface* 117: F02002. DOI: 10.1029/2011JF001975

Carbonneau PE, Lane SN Bergeron NE. 2004. Catchment-scale mapping of surface grain size in gravel bed rivers using airborne digital imagery. *Water Resources Research* 40: W07202. DOI: 10.1029/2003wr002759

Carling PA, Orr H, Kelsey A. 2006. The dispersion of magnetite bedload tracer across a gravel point-bar and the development of heavy-mineral placers. *Ore Geology Reviews* 28: 402-416. DOI: 10.1016/j.oregeorev.2005.02.003

Chagué-Goff C, Rosen MR. 2001. Using sediment chemistry to determine the impact of treated wastewater discharge on a natural wetland in New Zealand. *Environmental Geology* 40: 1411-1423. DOI: 10.1007/s002540100322

Chanson H 2004. *The Hydraulics of Open Channel Flow: An Introduction,* Oxford, UK: Elsevier Butterworth Heinemann.

Church M, Jones D. 1982. Channel bars in gravel bed rivers. In Hey RD, Bathurst JC, Thorne CR (eds.) *Gravel-bed Rivers: Fluvial Processes, Engineering, and Management.* Chichester: Wiley

Church M, Kellerhals R. 1978. On the statistics of grain size variation along a gravel river. *Canadian Journal of Earth Sciences* 15: 1151-1160

Church M, Rice SP. 2009. Form and growth of bars in a wandering gravel-bed river. *Earth Surface Processes and Landforms* 34: 1422-1432. DOI: 10.1002/esp.1831

Church M. 2010. Gravel-bed rivers. In Burt T, Allison R (eds.) *Sediment Cascades: An Integrated Approach.* Wiley: Chichester.

Coleman SE and Smart GM. 2011. Fluvial Sediment-transport Processes and Morphology. *Journal of Hydrology (New Zealand)* 50: 37-58.

Costa JE & O'Connor JE. 1995. Geomorphically Effective Floods. In Costa JE, Millar AJ, Potter KW, Wilcock PR (eds.) *Natural and Anthropogenic Influences in Fluvial Geomorphology: Geophysical Monograph 89.* Washington: American Geophysical Union

Cronin SJ, Neall VE, Palmer AS. 1997. Lahar history and lahar hazard of the Tongariro River, northeastern Tongariro Volcanic Centre, New Zealand. *New Zealand Journal of Geology and Geophysics* 40: 383-393

Doyle MW, Shields D, Boyd KF, Skidmore PB, Dominick D. 2007. Channel-Forming Discharge Selection in River Restoration Design. *Journal of Hydraulic Engineering* 133: 831-837

Environment Agency. 2013. *Benchmarking the latest generation of 2D hydraulic flood modelling packages*. Environment Agency Report SC120002, ISBN: 978-1-84911-306-9, Bristol, UK, https://www.gov.uk/government/publications/benchmarking-the-latest-generation-of-2d-hydraulic-flood-modelling-packages (Accessed September 2017).

Fagents, SA & Baloga, SM. 2005. Calculation of lahar transit times using digital elevation data. *Journal of Volcanology and Geothermal Research* 139: 135-146. DOI: 10.1016/j.jvolgeores.2004.06.013

Ferguson RI, Ashworth PJ. 1992. Spatial patterns of bedload transport and channel change in braided and near-braided rivers. In Billi P, Hey RD, Thorne CR, Tacconi P (eds.) *Dynamics of gravel-bed rivers.* Wiley: Chichester

Feurer D, Bailly JS, Puech C, Le Coarer Y, Viau AA. 2008. Very-high-resolution mapping of river-immersed topography by remote sensing. *Progress in Physical Geography* 32: 403-419. DOI: 10.1177/0309133308096030

Fryirs KA, Brierley GJ, Preston NJ, Kasai M. 2007. Buffers, barriers and blankets: The (dis)connectivity of catchment-scale sediment cascades. *Catena* 70: 49-67. DOI: 10.1016/j.catena.2006.07.007

Fryirs KA, Wheaton JM, Brierley GJ. 2016. An approach for measuring confinement and assessing the influence of valley setting on river forms and processes. *Earth Surface Processes and Landforms* 41: 701-710. DOI: 10.1002/esp.3893

Fuller IC, Large ARG, Milan DJ. 2003. Quantifying channel development and sediment transfer following chute cutoff in a wandering gravel-bed river. *Geomorphology* 54: 307-323. DOI: 10.1016/s0169-555x(02)00374-4

Genesis Energy. 2000. *Tongariro Power Development: Resource Consent Application and Assessment of Environmental Effects.* Turangi: Genesis Power Limited.

Graham DJ, Rice SP, Reid I. 2005. A transferable method for the automated grain sizing of river gravels. *Water Resources Research* 41: W07020. DOI: 10.1029/2004wr003868

Gray JR, Laronne JB, Marr JDG. 2010. *Bedload surrogate monitoring techniques.* U.S. Geological Surveys Report 2010-5091.

Guan M, Wright NG, Sleigh PA, Ahilan S, Lamb R. 2016. Physical complexity to model morphological changes at a natural channel bend, *Water Resources Research* 52: 6348–6364. DOI:10.1002/2015WR017917.

Habersack H, Nachtnebel H, Laronne J. 1998. The hydraulic efficiency of a slot sampler: flow velocity measurements in the Drau River, Austria. In Klingeman PC, Beschta RL, Komar PD, Bradley JB (eds.) *Gravel-Bed Rivers in the Environment.* Highland Ranch, CO: Water Resources Publications

Ham D, Church M. 2012. Morphodynamics of an extended bar complex, Fraser River, British Columbia. *Earth Surface Processes and Landforms* 37: 1074-1089. DOI: 10.1002/esp.3231

Hassan MA, Ergenzinger P. 2005. Use of Tracers in Fluvial Geomorphology. In Kondolf M, Piegay, H (Ed) *Tools in Fluvial Geomorphology.* Wiley: Chichester. DOI: 10.1002/0470868333.ch14

Heritage GL, Milan DJ. 2009. Terrestrial Laser Scanning of grain roughness in a gravel-bed river. *Geomorphology* 113: 4-11. DOI: 0.1016/j.geomorph.2009.03.021

Hicks DM, Gomez B. 2005. Sediment transport. In Kondolf G, Piegay H (eds.) *Tools in Fluvial Geomorphology.* Wiley: Chichester.

Hicks DM, Mason PD 1991. *Roughness Characteristics of New Zealand Rivers : A Handbook for Asigning Hydraulic Roughness Coefficients to River Reaches by the "Visual Comparison" Approach* Water Resources Survey, DSIR Marine and Freshwater: Wellington.

Hodge RA, Brasington J, Richards K. 2009. Analysing laser-scanned digital terrain models of gravel bed surfaces: linking morphology to sediment transport

processes and hydraulics. *Sedimentology* 56: 2024-2043. DOI: 10.1111/j.1365-3091.2009.01068.x

Hodge RA, Sear DA, Leyland J. 2013. Spatial variations in surface sediment structure in riffle–pool sequences: a preliminary test of the Differential Sediment Entrainment Hypothesis (DSEH). *Earth Surface Processes and Landforms* 38: 449-465. DOI: 10.1002/esp.3290

Hoyle J, Brierley G, Brooks A, Fryirs K. 2007. Sediment organisation along the upper Hunter River, Australia: a multivariate statistical approach. In Habersack HP, Massimo R (eds.) *Gravel-Bed Rivers VI: From Process Understanding to River Restoration.* Elsevier: Oxford; 409-442

Hoyle JT, Kilroy C, Hicks DM, Brown L. 2017. The influence of sediment mobility and channel geomorphology on periphyton abundance. *Freshwater Biology* 62: 258-273. DOI: 10.1111/fwb.12865

Jolly AD, Jousset P, Lyons JJ, Carniel R, Fournier N, Fry B, Miller C. 2014. Seismo-acoustic evidence for an avalanche driven phreatic eruption through a beheaded hydrothermal system: An example from the 2012 Tongariro eruption. *Journal of Volcanology and Geothermal Research* 286: 331-347. DOI: http://dx.doi.org/10.1016/j.jvolgeores.2014.04.007

Keulegan GH. 1938. Laws of turbulent flow in open channels. *Journal National Bureau of Standards.* Research Paper 1151, 21: 707-741, Washington, D.C.

Kilgour G, Manville V, Pasqua FD, Graettinger A, Hodgson KA, Jolly GE. 2010. The 25 September 2007 eruption of Mount Ruapehu, New Zealand: Directed ballistics, surtseyan jets, and ice-slurry lahars. *Journal of Volcanology and Geothermal Research* 191: 1-14. DOI: http://dx.doi.org/10.1016/j.jvolgeores.2009.10.015

Knighton D. 1998. *Fluvial forms and processes: A new perspective.* Edward Arnold: London

Kondolf GM, Lisle TE, Wolman GM. 2005. Bed sediment measurement. In Kondolf G, Piegay H (eds.) *Tools in Fluvial Geomorphology.* Wiley: Chichester

Laronne JB, Duncan MJ. 1992. Bedload transport paths and gravel bed formaiton. In Billi P (ed.) *Dynamics of Gravel-bed Rivers.* Chichester: Wiley; 177-202

Laronne JB, Garcia C, Reid I. 2001. Mobility of patch sediment in gravel bed streams: patch character and its implications for bedload. In Mosley, MP (ed.) *Gravel Bed Rivers V.* Wellington: New Zealand Hydrological Society; 249-289

Legleiter CJ, Roberts DA, Marcus, WA & Fonstad, MA. 2004. Passive optical remote sensing of river channel morphology and in-stream habitat: Physical basis and feasibility. *Remote Sensing of Environment* 93: 493-510. DOI: http://dx.doi.org/10.1016/j.rse.2004.07.019

Lenzi MA, Mao L, Comiti F. 2006. Effective discharge for sediment transport in a mountain river: Computational approaches and geomorphic effectiveness. *Journal of Hydrology* 326: 257-276. DOI: 10.1016/j.jhydrol.2005.10.031

Leopold LB, Wolman GM, Miller, J 1964. *Fluvial Processes in Geomorphology,* New York: Dover Publications..

Lunt IA, Bridge JS. 2004. Evolution and deposits of a gravelly braid bar, Sagavanirktok River, Alaska. *Sedimentology* 51: 415-432. DOI: 10.1111/j.1365-3091.2004.00628.x

Lyzenga DR. 1981. Remote sensing of bottom reflectance and water attenuation parameters in shallow water using aircraft and Landsat data. *International Journal of Remote Sensing* 2: 71-82. DOI: 10.1080/01431168108948342

Mackenzie LG, Eaton BC. 2017. Large grains matter: contrasting bed stability and morphodynamics during two nearly identical experiments. *Earth Surface Processes and Landforms* 42: 1287-1295. DOI: 10.1002/esp.4122

Magilligan FJ. 1992. Thresholds and the spatial variability of flood power during extreme floods. *Geomorphology* 5: 373-390. DOI: 10.1016/0169-555X(92)90014-F

Mao L, Surian N. 2010. Observations on sediment mobility in a large gravel-bed river. *Geomorphology* 114: 326-337. DOI: 10.1016/j.geomorph.2009.07.015

Mao L, Dell'Agnese A, Comiti F, 2017. Sediment motion and velocity in a glacier-fed stream. *Geomorphology* 291: 69-79. DOI: 10.1016/j.geomorph.2016.09.008

Marutani T, Kasai M, Reid LM, Trustrum NA. 1999. Influence of storm-related sediment storage on the sediment delivery from tributary catchments in the upper Waipaoa River, New Zealand. *Earth Surface Processes and Landforms* 24: 881-896

Nakagawa M, Wada K, Thordarson T, Wood CP, Gamble JA. 1999. Petrologic investigations of the 1995 and 1996 eruptions of Ruapehu volcano, New Zealand: formation of discrete and small magma pockets and their intermittent discharge. *Bulletin of Volcanology* 61: 15-31. DOI: 10.1007/s004450050259

Passalacqua P, Belmont P, Staley DM, Simley JD, Arrowsmith JR, Bode CA, Crosby C, Delong SB, Glenn NF, Kelly SA, Lague D, Sangireddy H, Schaffrath K, Tarboton DG, Wasklewicz T, Wheaton JM. 2015. Analyzing high resolution topography for advancing the understanding of mass and energy transfer through landscapes: A review. *Earth-Science Reviews* 148: 174-193. DOI: 10.1016/j.earscirev.2015.05.012

Pasternack GB, Gilbert AT, Wheaton JM, Buckland EM. 2006. Error propagation for velocity and shear stress prediction using 2D models for environmental management. *Journal of Hydrology* 328: 227-241. DOI: 10.1016/j.jhydrol.2005.12.003

Pearson E, Smith MW, Klaar MJ, Brown LE. 2017. Can high resolution 3D topographic surveys provide reliable grain size estimates in gravel bed rivers? *Geomorphology* 293: 143-155. DOI: http://dx.doi.org/10.1016/j.geomorph.2017.05.015

Phillips JD. 2002. Geomorphic impacts of flash flooding in a forested headwater basin. *Journal of Hydrology* 269: 236-250. DOI: 10.1016/s0022-1694(02)00280-9

Reid HE, Brierley GJ. 2015. Assessing geomorphic sensitivity in relation to river capacity for adjustment, *Geomorphology* 250: 108 – 121

Reid HE, Brierley GJ, McFarlane K, Coleman SE, Trownsdale S. 2013. The role of landscape setting in minimizing hydrogeomorphic impacts of flow regulation, *International Journal of Sediment Research* 28: 149 – 161. DOI: 10.1016/j.geomorph.2015.09.009

Rennie CD, Church M. (2010), Mapping spatial distributions and uncertainty of water and sediment flux in a large gravel bed river reach using an acoustic Doppler current profiler, *Journal of Geophysical Research - Earth Surface* 115: F03035. DOI: 10.1029/2009jf001556.

Rennie CD, Millar RG. 2000. Spatial variability of stream bed scour and fill: a comparison of scour depth in chum salmon (Oncorynchus keta) redds and adjacent bed. *Canadian Journal of Fisheries and Aquatic Sciences* 57: 928-938.

Rice SP, Church M. 2010. Grain-size sorting within river bars in relation to downstream fining along a wandering channel. *Sedimentology* 57: 232-251. DOI: 10.1111/j.1365-3091.2009.01108.x

Rice SP, Church M, Wooldridge CL, Hickin EJ. 2009. Morphology and evolution of bars in a wandering gravel-bed river; lower Fraser river, British Columbia, Canada. *Sedimentology* 56: 709-736. DOI: 10.1111/j.1365-3091.2008.00994.x

Rodrigues S, Claude N, Juge P, Breheret J-G. 2012. An opportunity to connect the morphodynamics of alternate bars with their sedimentary products. *Earth Surface Processes and Landforms* 37: 240-248. DOI: 10.1002/esp.2255

Roe PL, Pike J. 1984. Efficient construction and utilisation of approximate Riemann solutions. In: Glowinski, R. and Lions, J.L. (Eds). *Proc. of the Sixth Int. Symposium on Computer Methods in Applied Sciences and Engineering*, 499-518, Amsterdam: North-Holland.

Rosen MR, Chagué-Goff C, Eser P, Coshell L. 2002. Utilisation of the sedimentological and hydrochemical dynamics of the Stump Bay Wetland along Lake Taupo, New Zealand, for the recognition of paleo-shoreline indicators. *Sedimentary Geology* 148: 357-371. DOI: 10.1016/s0037-0738(01)00226-3

Rubin DM. 2004. A Simple Autocorrelation Algorithm for Determining Grain Size from Digital Images of Sediment. *Journal of Sedimentary Research* 74: 160-165. DOI: 10.1306/052203740160

Sambrook Smith GH, Best JL, Ashworth PJ, Lane SN, Parker NO, Lunt IA, Thomas RE, Simpson CJ. 2010. Can we distinguish flood frequency and magnitude in the sedimentological record of rivers? *Geology* 38: 579-582. DOI: 10.1130/g30861.1

Schneider JM, Rickenmann D, Turowski JM, Kirchner JW. 2015. Self-adjustment of stream bed roughness and flow velocity in a steep mountain channel. *Water Resources Research* 51: 7838-7859. DOI: 10.1002/2015WR016934

Shields A. 1936. *Anwendung der Aehnlichkeitsmechanik und der Turbulenz Forschung auf die Geschiebebewegung,* Berlin, Mitteilungen der Preussische Versuchanstalt für Wasserbau und Schiffbau.

Smart GM 1999. Lower Tongariro flooding and erosion study. Christchurch: NIWA Client Report CHC99/49 for Genesis Energy.

Soulsby RL, Whitehouse RJS. 1997. *Threshold of Sediment Motion in Coastal Environments*, Christchurch, N.Z.: Centre for Advanced Engineering, University of Canterbury.

Storz-Peretz Y, and Laronne JB. 2018, The morpho-textural signature of large bedforms in ephemeral gravel-bed channels of various planforms. *Hydrological Processes* 32: 617-635. DOI: 10.1002/hyp.11437.

Surian N, Mao L, Giacomin M, Ziliani L. 2009. Morphological effects of different channel-forming discharges in a gravel-bed river. *Earth Surface Processes and Landforms* 34: 1093-1107. DOI: 10.1002/esp.1798

Tarolli P. 2014. High-resolution topography for understanding Earth surface processes: Opportunities and challenges. *Geomorphology* 216: 295-312. DOI: 10.1016/j.geomorph.2014.03.008

Tenzer R, Sirguey P, Rattenbury M, Nicolson J. 2011. A digital rock density map of New Zealand. *Computers and Geosciences* 37: 1181-1191. DOI: 10.1016/j.cageo.2010.07.010

Toro EF. 2001. *Shock–Capturing Methods for Free-Surface Shallow Flows*. Chichester: Wiley. 326 pp.

Vázquez-Tarrío D, Borgniet L, Liébault F, Recking A. 2017. Using UAS optical imagery and SfM photogrammetry to characterize the surface grain size of gravel bars in a braided river (Vénéon River, French Alps). *Geomorphology* 285: 94-105. DOI: http://dx.doi.org/10.1016/j.geomorph.2017.01.039

Verdú JM, Batalla RJ, Martínez-Casasnovas JA. 2005. High-resolution grain-size characterisation of gravel bars using imagery analysis and geo-statistics. *Geomorphology* 72: 73-93. DOI: 10.1016/j.geomorph.2005.04.015

Westoby MJ, Dunning SA, Woodward J, Hein AS, Marrero SM, Winter K, Sugden DE. 2015. Sedimentological characterization of Antarctic moraines using UAVs and Structure-from-Motion photogrammetry. *Journal of Glaciology* 61: 1088-1102. DOI: 10.3189/2015JoG15J086

Wheaton JM, Brasington J, Darby SE, Kasprak A, Sear D, Vericat D. 2013. Morphodynamic signatures of braiding mechanisms as expressed through change in sediment storage in a gravel-bed river. *Journal of Geophysical Research: Earth Surface* 118: 759-779. DOI: 10.1002/jgrf.20060

Wheaton JM, Fryirs KA, Brierley G, Bangen SG, Bouwes N, O'Brien G. 2015. Geomorphic mapping and taxonomy of fluvial landforms. *Geomorphology* 248: 273-295. DOI: 10.1016/j.geomorph.2015.07.010

Wilcock P, Pitlick J, Cui Y. 2009. *Sediment transport primer: estimating bed-material transport in gravel-bed rivers.* U.S. Department of Agriculture, Forest Service.

Williams GP. 1978. Bank-full discharge of rivers. *Water Resourses Research* 14: 1141-1154. DOI: 10.1029/WR014i006p01141

Williams RD, Brasington J, Vericat D, Hicks DM, Labrosse F, Neal M. 2011. Monitoring braided river change using terrestrial laser scanning and optical bathymetric

mapping. In Smith, M, Paron, P and Griffiths, J (eds.) *Geomorphological Mapping: Methods and Applications.* USA: Elsevier Science and Technology

Williams RD, Brasington J, Hicks M, Measures R, Rennie CD and Vericat D. 2013. Hydraulic validation of two-dimensional simulations of braided river flow with spatially continuous aDcp data. *Water Resources Research* 49: 5183-5205. DOI: 10.1002/wrcr.20391

Williams RD, Brasington J, Vericat D, Hicks DM. 2014. Hyperscale terrain modelling of braided rivers: fusing mobile terrestrial laser scanning and optical bathymetric mapping. *Earth Surface Processes and Landforms* 39: 167-183. DOI: 10.1002/esp.3437

Williams RD, Rennie CR, Brasington J, Hicks DM, Vericat D. 2015. Within-event spatially distributed bed material transport: linking apparent bedload velocity to morphological change. *Journal of Geophysical Research: Earth Surface* 120: 604-622. DOI: 10.1002/2014JF003346

Wilson CJN, Walker GPL. 1985. The Taupo Eruption, New Zealand I. General Aspects. *Philosophical Transactions of the Royal Society of London. Series A, Mathematical and Physical Sciences* 314: 199-228. DOI: 10.1098/rsta.1985.0019

Wohl E, Bledsoe BP, Jacobson RB, Poff NL, Rathburn SL, Walters DM, Wilcox, AC. 2015. The Natural Sediment Regime in Rivers: Broadening the Foundation for Ecosystem Management. *BioScience* 65: 358-371. DOI: 10.1093/biosci/biv002

Wolman GM. 1954. A method of sampling coarse river-bed material. *Transactions of the American Geophysical Union* 35: 951-956

Wolman M, Miller J. 1960. Magnitude and frequency of forces in geomorphic processes. *Journal of Geology* 68: 54–74

Wolman MG, Gerson R. 1978. Relative scales of time and effectiveness of climate in watershed geomorphology. *Earth Surface Processes* 3: 189-208. DOI: 10.1002/esp.3290030207

Woodget AS, Austrums R. 2017. Subaerial gravel size measurement using topographic data derived from a UAV-SfM approach. *Earth Surface Processes and Landforms* 42: 1434-1443. DOI: 10.1002/esp.4139

Table 1 Characteristics of each bar.

Bar name	Blue	Red Hut	Breakfast	Bain
Distance downstream[a]	57.63	60.44	65.15	68.04
Bar area (m^2)	2163	7775	4374	4641
Valley width (m)	246	80[b]	80	Unconfined
D_{50} (mm)[c]	230	140	113.5	84.5
Slope[d]	0.008	0.005	0.003	0.003
River Style	Partly confined, wandering, cobble	Partly confined, wandering, cobble	Partly confined, wandering, cobble	Unconfined, braided, gravel
Process zone	Transfer	Transfer	Transfer	Accumulation
Terrace height	25 m	12 m	7 m	None

[a] Distance downstream from the most upstream drainage point in the catchment.
[b] Red Hut is located at a localised pinch in the valley. The channel width is up to 1 km upstream and 250 m downstream.
[c] 100 Wolman clasts sampled at the coarsest locale of the bar.
[d] Water surface slope extracted from 1 m resolution airborne LiDAR data.

Table 2 Description of geomorphic units used to define the different morphological and sediment characteristics across the bar surfaces. These are based on units described by Bluck (1982; 1971).

Bar unit	Morphological and sediment distribution characteristics	Process-form relationship
Bar head	Coarsest locale of the bar commonly found at the bar head or on the apex of bends next to the channel. Surface commonly slopes up to meet the flatter supra-platform.	This unit is scoured during high flow, representing the highest energy environment. It may be an extension of a coarse riffle located in the wetted channel.
Supra-platform	Middle, flatter section of the bar, between the bar head and bar tail, which is essentially the bar top. Commonly exhibits a downstream fining trend in grain-size (Rice and Church, 2010). Bars which exhibited pronounced downstream fining within this unit were separated into upstream (US) and downstream (DS) supra-platform units.	Comprises the main bulk of the deposit which is protected by the bar head and has comparatively lower shear stress during floods. May have vegetation starting to colonise more protected sections which can create topographic irregularities. Preferential pathways of flow can also carve out lower zones with coarser sediment.
Bar tail	Depositional feature at the downstream extent of the bar which is made up of smaller grains often predominantly coarse gravel within this system, with some sand deposits.	This unit is protected by the coarser, higher elevation deposit upstream. Smaller grains are deposited here during the falling limb of floods.
Back channel	Channel which is cut around the back of the bar and only inundated during high flow. This surface is lower than the adjacent supra-platform and may have fines superimposed which are captured during the falling limb of floods.	During floods, flow scours the channel. In wandering gravel-bed rivers this channel may have been a previous primary channel which has become depositional as a mid-channel bar has transitioned to a lateral bar.
Fine-grained deposit	Localised area of fines or smaller clasts deposited on the bar at a location which is not the tail. This was sometimes observed at the upstream location of the bar when the larger material of the bar head was located at the apex of the bar rather than the upstream section.	Localised protected areas cause a depositional environment to form within the bar surface.

Table 3 Recurrence Intervals and Annual Exceedence Probabilities for different flood events, based on 50 years of discharge data measured at the Tongariro at Turangi Flow gauging station.

Recurrence Interval of the flood (RI) (years)	**Notation used in the text to describe flood**	**Discharge *(m^3s^{-1})***	**Annual Exceedence Probability (AEP) *(%)***
2.33	Q2.33	480	50
10	Q10	850	10
20	Q20	1000	5
50	Q50	1250	2
100	Q100	1500	1

Table 4 Error statistics from a comparison between flow model predictions and aDcp observations, based upon 6,470 aDcp measurements. Formulae for error statistics can be found in Table 3 of Williams et al. (2014).

Error statistic	**Depth, m**	**Velocity, ms^{-1}**
Mean Error	-0.045	0.129
Standard Deviation Error	0.055	0.202
Mean Absolute Error	0.056	0.194
Root Mean Squared Error	0.071	0.239

Table 5 Grain-size and area characteristics of within bar geomorphic units and the percentage of sediment entrainment on each unit and bar during different magnitude/frequency flood events. The location of geomorphic units superimposed on each bar is shown in Figure 4.

	Unit	Area, m^2	% of bar area	Average D_{50}, mm	Grain-size classification	Percentage of each unit entrained during each flood event				
						Q2.33 480 m^3s^{-1}	***Q10 850 m^3s^{-1}***	***Q20 1000 m^3s^{-1}***	***Q50 1250 m^3s^{-1}***	***Q 1 m***
	Head	792	41	214	Coarse cobble	10	43	63	91	
	Supra-platform	291	15	171	Coarse cobble	46	83	81	91	1
	Back channel	504	26	132	Coarse cobble	28	59	64	85	
	Tail	365	19	74	Cobble	74	98	99	99	
Total Bar Entrainment						**33**	**64**	**73**	**91**	
lut	Head	978	15	173	Coarse cobble	21	21	21	21	
	US supra-platform*	1928	29	128	Cobble	37	39	39	39	
	DS supra-platform*	1804	27	110	Cobble	6	12	14	16	
	Back channel	1058	16	78	Cobble	10	14	15	20	
	Tail	809	12	36	Very coarse gravel	68	81	84	88	
Total Bar Entrainment						**26**	**30**	**31**	**33**	
kfa	Head	1577	40	143	Coarse cobble	18	47	53	70	
	Supra-platform	1318	34	101	Cobble	6	36	46	61	
	Tail	760	20	22	Coarse gravel	81	94	96	99	
Total Bar Entrainment						**26**	**52**	**59**	**73**	
	Head	1251	33	67	Cobble	3	11	11	12	
	Supra-platform	810	21	42	Very coarse gravel	13	35	36	36	
	Back channel	883	23	21	Coarse gravel	41	68	71	73	
	Tail	684	18	46	Very coarse gravel	11	33	35	35	
Total Bar Entrainment						**15**	**33**	**34**	**35**	

* The supra-platform of Red Hut bar was large and exhibited marked downstream fining so was separated into two different units, the US (upstream) and DS (downstream) supra platforms.

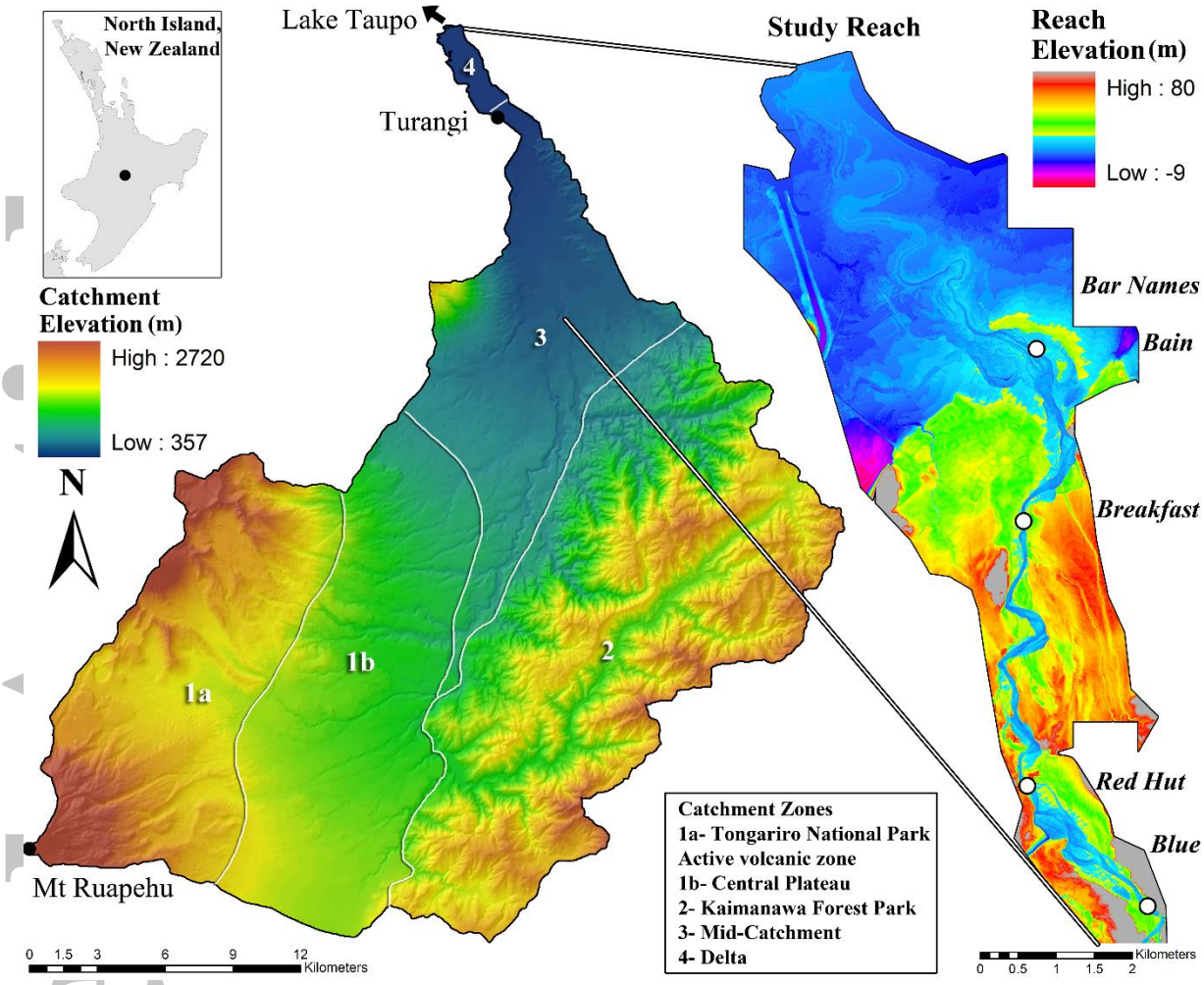

Figure 1 Location map of the Tongariro Catchment. Landscape attributes of each zone are outlined in the text. The DEM for the study reach was derived from 1 m airborne LiDAR data which has been detrended to remove the influence of slope. This allows greater appreciation of lateral heights of features above the water surface. Bars surveyed within this paper are annotated.

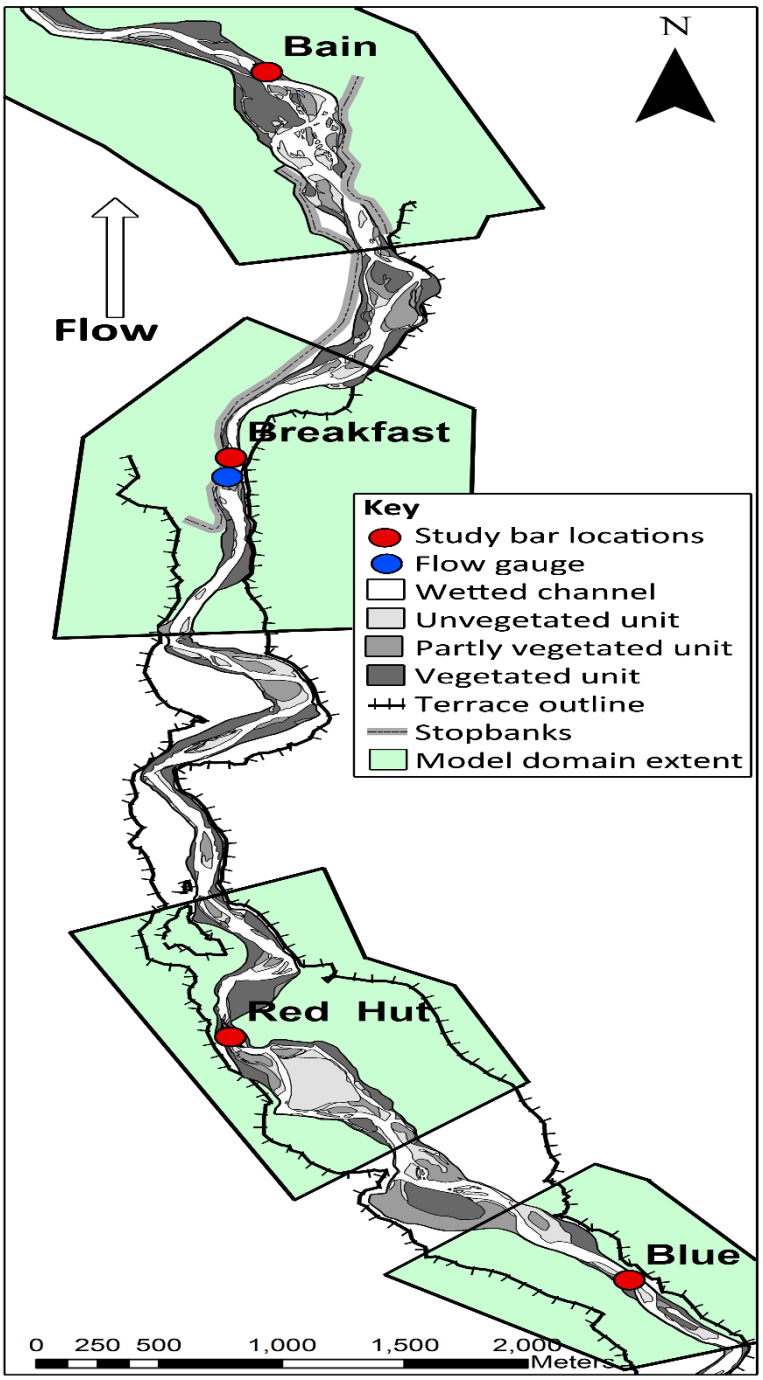

Figure 2 Location of study bars and JFlow® model domains, superimposed upon the 2007 channel outline. The terrace outline width indicates the zone that has undergone incision following the Taupo eruption (1.8 ka). At some locations, such as at Red Hut, contemporary valley width is narrower.

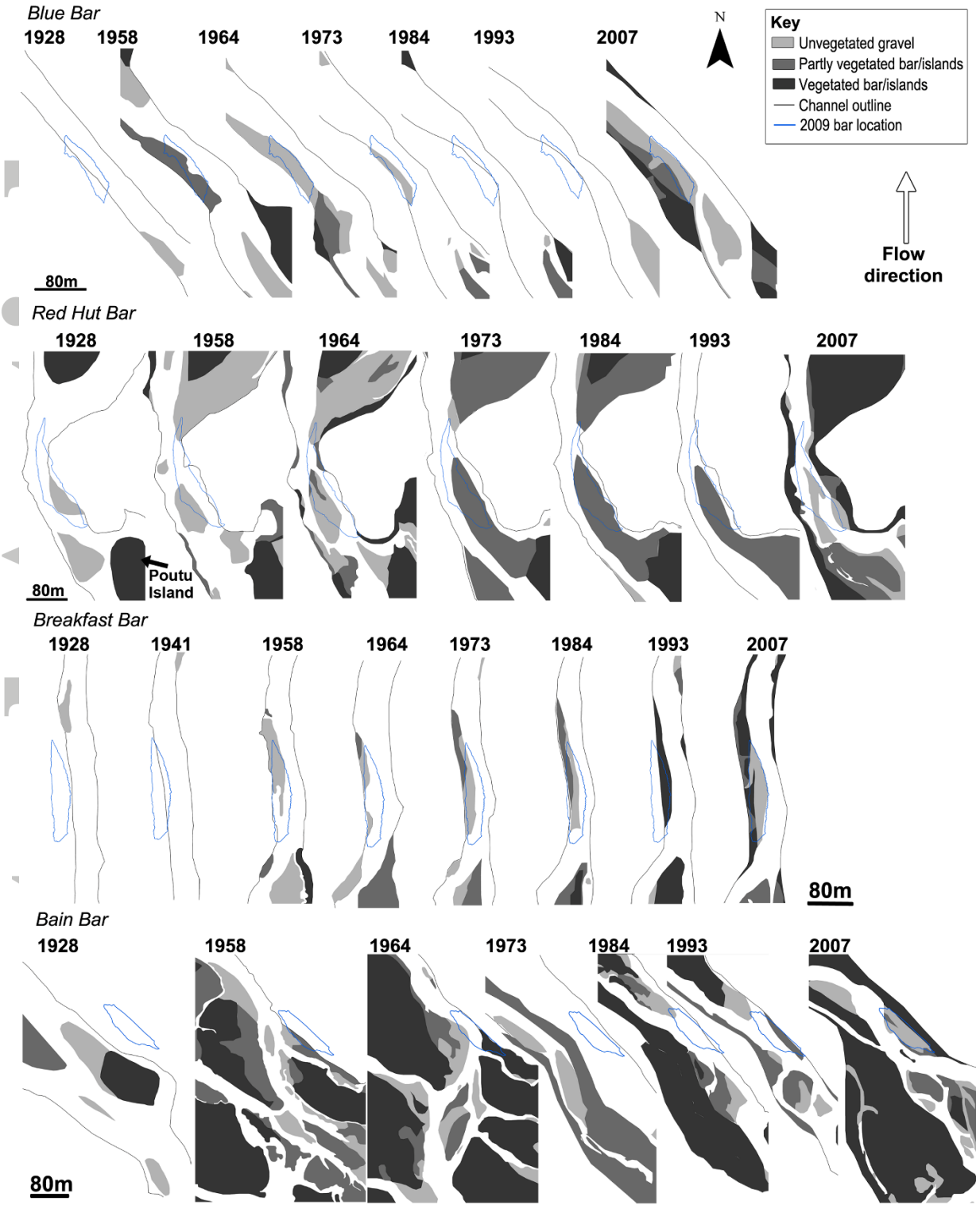

Figure 3 Bar development extracted from aerial photography (1941 – 2007) and a survey map (1928). Note: as the 1928 image was derived from a survey map, it has greater error and imprecision with regards to the placement and dimensions of the units relative to the other images.

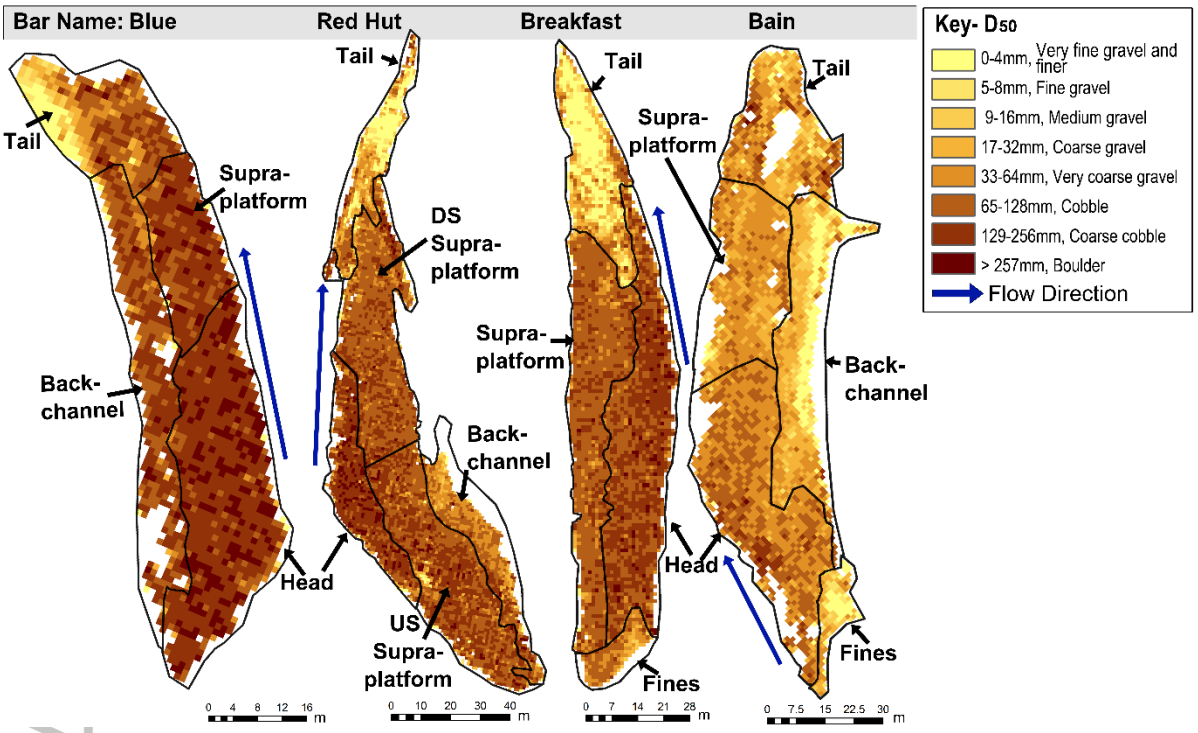

Figure 4 Map showing within bar geomorphic units and the distribution of grain-size across the bar surfaces as derived from a correlation between median grain size and TLS detrended standard deviation (Figure 5). Placement left to right represents the downstream progression of bars.

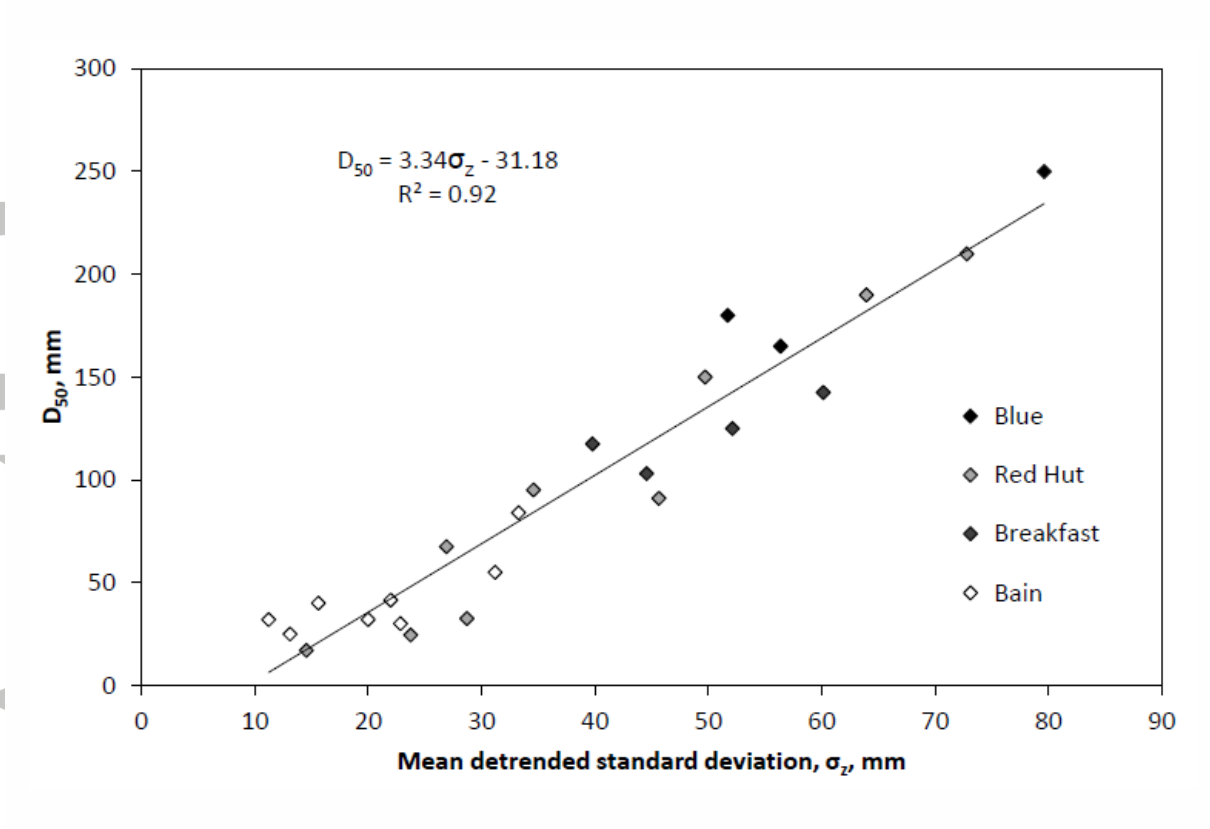

Figure 5 Correlation between median grain-size (D_{50}) and TLS detrended standard deviation (σ_z) for 1 m^2 patches, averaged across the area covered by the D_{50} Wolman transects. The resulting linear relationship was used to convert maps of σ_z to grain-size at a 1 m^2 scale across all four bars.

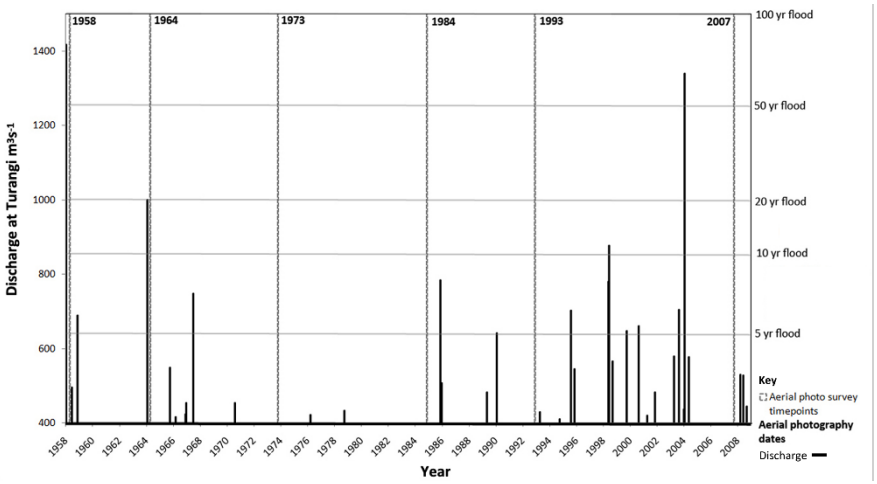

Figure 6 Distribution of flood events with discharge > 400 m^3s^{-1} since 1958 for the Tongariro River at Turangi flow gauge. Vertical dotted lines indicate aerial photograph surveys which coincide with the images in Figure 3 and the horizontal lines indicate the recurrence interval for different discharge events.

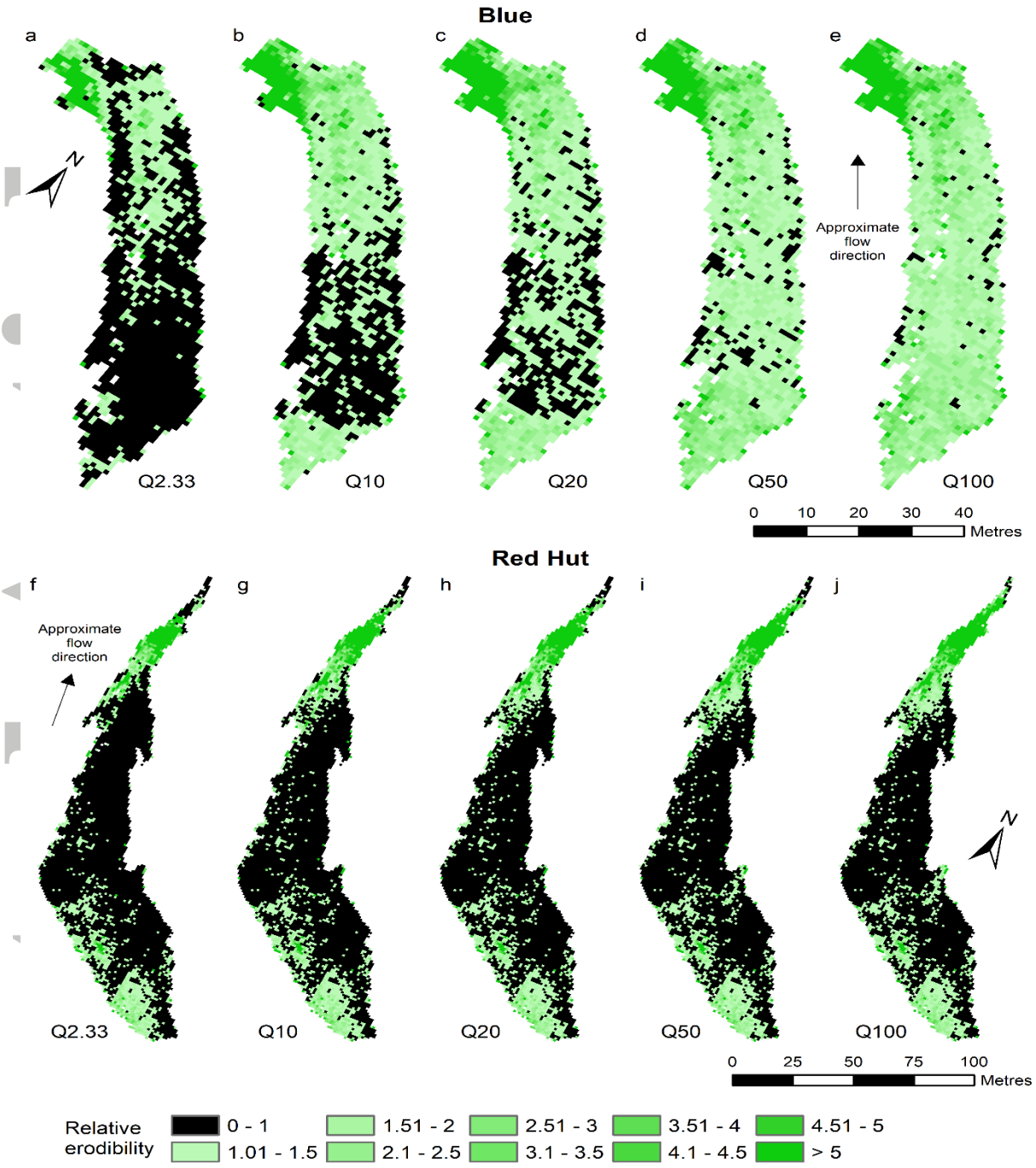

Figure 7 Relative erodibility calculated by the ratio of dimensionless shear stress to critical shear stress at a 1 m^2 resolution for the two most upstream bars, Blue bar (a to e) and Red Hut bar (f to j), for five flood events. Black shading indicates any value less than 1, where sediment remains immobile. Excess shear stress above this threshold is expressed in the colour continuum from light (lower excess shear stress) to dark (very high excess shear stress) green.

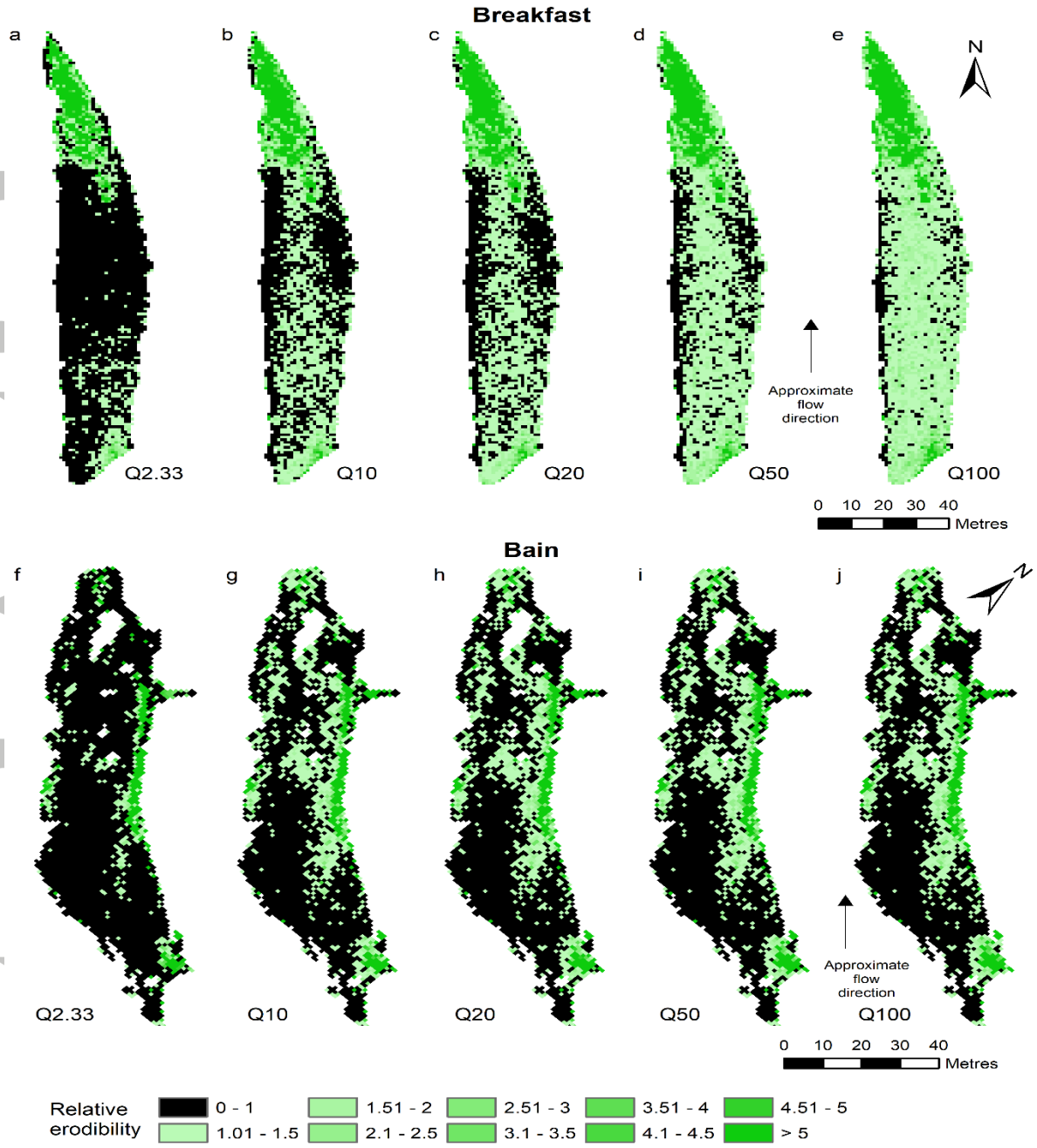

Figure 8 Relative erodibility calculated by the ratio of dimensionless shear stress to critical shear stress at a 1 m^2 resolution for the two most downstream bars, Breakfast bar (a to e) and Bain bar (f to j), for five flood events. Black shading indicates any value less than 1, where sediment remains immobile. Excess shear stress above this threshold is expressed in the colour continuum from light (lower excess shear stress) to dark (very high excess shear stress) green.

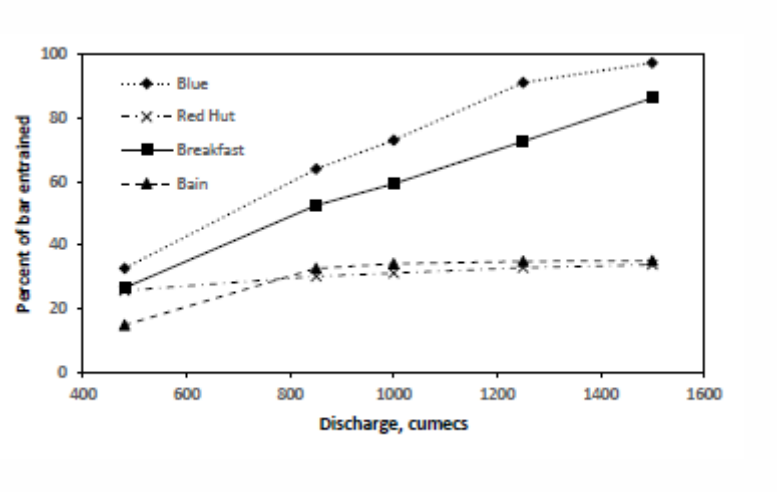

Figure 9 The percentage of each bar reworked by different magnitude/frequency flood events.

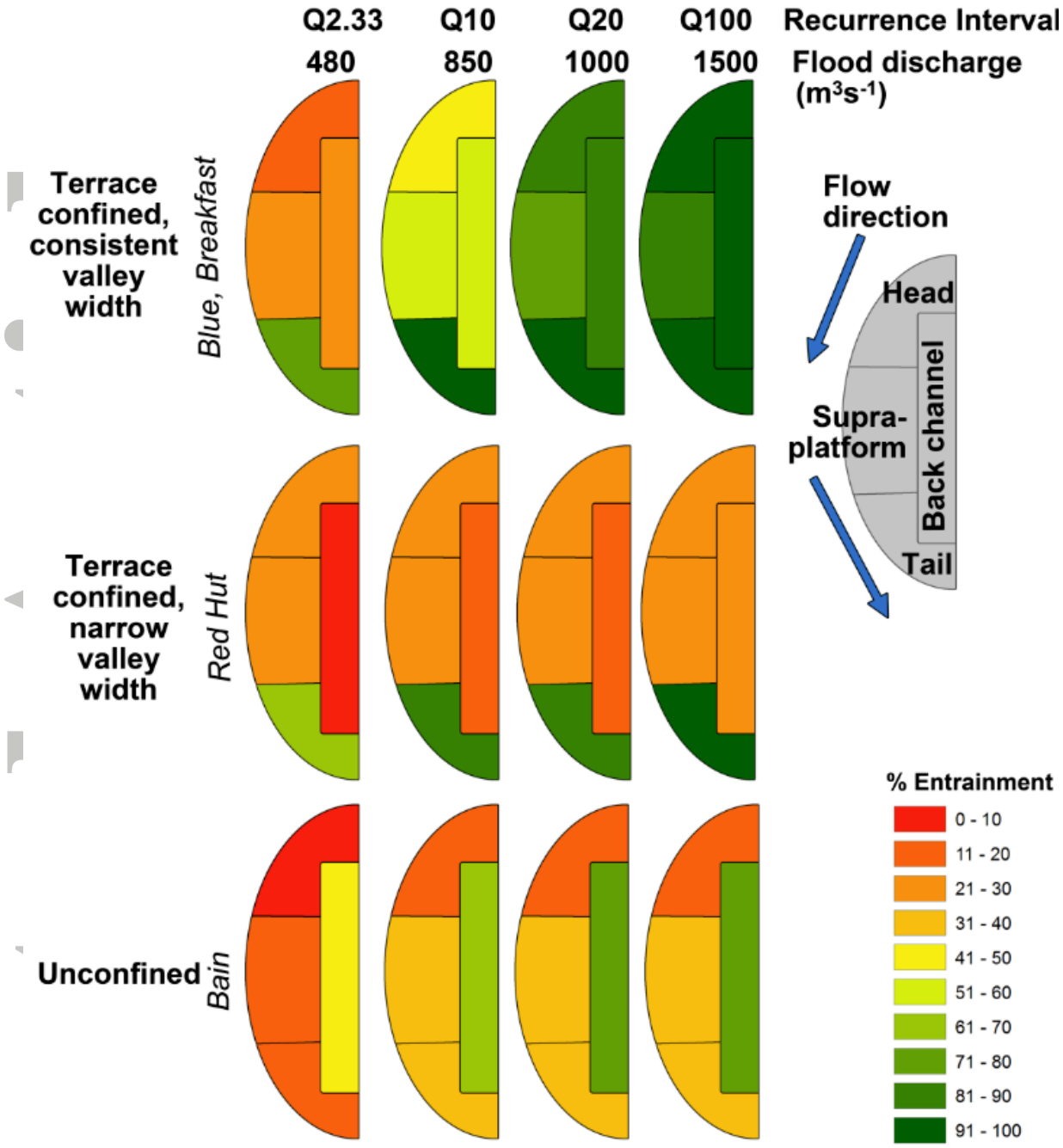

Figure 10 Conceptual model of the proportion of each bar unit reworked by different magnitude flood events, within each zone of the river.